NOVA SCHOOL OF SCIENCE & TECHNOLOGY

DEPARTAMENT OF MATERIALS SCIENCE

MARIANA FILIPA DE ABREU ALVES

Bachelor of Science in Micro and Nanotechnology Engineering

Design and fabrication of microgel shapes as red blood cell substitutes (RBCs) by UV-assisted punching

MASTER OF SCIENCE IN MICRO AND NANOTECHNOLOGY ENGINEERING

NOVA University of Lisbon

October, 2022

NOVA SCHOOL OF
SCIENCE & TECHNOLOGY

DEPARTAMENT OF MATERIALS SCIENCE

Design and fabrication of microgel shapes as red blood cell substitutes (RBCs) by UV-assisted punching

MARIANA FILIPA DE ABREU ALVES

Bachelor of Science in Micro and Nanotechnology Engineering

Adviser: Stephan Sylvest Keller
Full Professor, Technical University of Denmark

Co-adviser: João Paulo Miranda Ribeiro Borges
Associate Professor, NOVA University Lisbon

MASTER OF SCIENCE IN MICRO AND NANOTECHNOLOGY

NOVA University Lisbon
<October>, <2022>

Design and fabrication of microgel shapes as red blood cells substitutes (RBCs) by UV-assisted punching

For my mom.

ACKNOWLEDGMENTS

This thesis is a representation of the end of a big era in my life. It is an important mark in my education, however, it is an even greater mark in my personal life. As I have spent five years building friendships and making memories that will last me for a lifetime. But before getting into that I would like to take a moment to thank my home university, FCT, for these years of education and opportunities. For all the teachers and classes that had an impact on me. For all the moments I felt inspired and capable and even for the moments, I felt unmotivated and hopeless. The inspired moments made me think outside of the box, be creative in my critical thinking, and attempt new things that otherwise I would not have. The unmotivated problems contributed greatly for my personal growth, they taught me that even in your worst moment there is always a way through. In addition, I would like to specifically thank to Professor Elvira Fortunato and Rodrigo Martins who created this degree. Perhaps even without knowing that it they were changing forever the lives of so many students and to more to come. Now to the university that welcomed me for this project, DTU, I have nothing but compliments to express, regardless of how challenging the project may have been for me. To Stephan, my adviser, I am incredibly thankful for the opportunity. More even for the way you welcomed me so easily into your research group BioMic, which offer me nothing but help and inspiration. Thanks also to my second research group, Health Tech, for transmitting to me a familiar feeling. Thank you, Stephan, again for being such a genuinely kind person, along with smart which made me feel safe and scientifically supported at once. To my co-adviser, Shahana, I would also like to give a special thanks, as she was the one that most dealt with me closely. For your astute intelligence and for pushing me to realize my potential, even when I was being negative. Thank you both in general as without you I would not have gotten this far.

Next to the people that stood and stand by me through life, I would like to give the greater round of applause for all the patience and dedication in keeping me above water. Only gratitude for you. Firstly, to my friend Eva, for always having a positive mindset and for sharing with me and marking this DTU experience. To my longest faithful best friends, Constança and Raquel, thank you for everything, but mostly for the help finishing this thesis, motivating me through it all. To my besties at FCT, Maria, Inês, Bia, Didi, Luna, David and Claudia, thank you for never giving up on me and for fully supporting me over these five years. You guys are now family. To my biological family, my mom, and my cousins, Rita, João and Tomás, thanks for being my straight-up rock, I would be nowhere without you. If finishing this thesis is a win, then it is for you and because of you. Lastly, but for sure not less important, thanks to you, Filipe, I cannot even put into words how lucky I am to have you in my life. You make me a better person in all senses, you help me unconditionally, and without your love and support I would struggle to keep pushing in this crazy life. Specifically, thanks for making dinner right now, as I finish this. It smells really good.

All good vibes here, see you all on the other side.

"*Hardships often prepare ordinary people*
for an extraordinary destiny"
(C.S. Lewis).

ABSTRACT

There is a constant high demand for blood transfusions worldwide. Donor-derived blood employed as the current clinical standard has several limitations including insufficient availability, short shelf-life, and risk of pathogenic contamination. Thus, the development of artificial red blood cells (RBCs) has become a crucial field of study. Such artificial RBCs encapsulate hemoglobin (Hb), the oxygen-carrying component of RBCs, and aim to mimic the features of the endogenous cells.

Currently, mainly microparticles and nanoparticles are used as encapsulated systems in drug delivery research. Polyethylene glycol (PEG)-based hydrogels are the primary choice for material, due to their biocompatibility. So far, most carriers developed have spherical shapes and are produced from bottom-up approaches that cannot offer the best geometric control. It has been proven that geometry plays a critical role in the vascular behavior of microparticles, thus the need to obtain non-spherical carriers.

This project proposed to employ top-down fabrication methods to better overcome this challenge. By aiming to design and fabricate three different PEG-based microgel shapes (rods, stars, and hexagons) designed within the same size range as RBCs. Firstly, Silicon masters with the designed patterns were produced through photolithography and dry etching. Then they were used to produce cyclo olefin polymer (COP) stamps through hot embossing. These stamps were coated with different PEG formulations (with and without Hb) by slot die coating. Next, they were used in UV-assisted punching to form the microgel shapes and mechanically punch through the hydrogel flash layer onto a poly-vinyl alcohol (PVA) substrate. The microgels were harvested by dissolving the PVA. These microgels shapes obtained had the desired aspect ratio of 3:1 retaining good shape features. However, challenges remained in the achievement of individual microgel shapes after harvest. Due to coating thickness limitations that consequently affected the mechanically punching process afterwards.

Keywords: artificial red blood cells (RBCs), poly(ethylene glycol) (PEG), silicon masters, cyclo Olefin polymer (COP) stamps, microgel shapes, slot die coating, UV-assisted punching.

Resumo

Existe uma constante procura de transfusões sanguíneas. Isto devido ao sangue proveniente de dadores ter inúmeras limitações incluindo disponibilidade insuficiente, baixa longevidade e risco de contaminação patogénica. Assim sendo o desenvolvimento de hemácias artificiais tornou-se um crucial ramo de investigação. Estas hemácias artificiais encapsulam a hemoglobina, componente transportador de oxigénio, visando imitar as características das células endógenas.

Atualmente maioritariamente micropartículas e nanopartículas são usadas como sistemas de encapsulamento em estudos de entrega de fármacos. Sendo os hidrogéis à base de polietilenoglicol (PEG) a maior escolha como material, devido à sua biocompatibilidade. Até agora, a maioria dos portadores desenvolvidos tem formas esféricas e são produzidos a partir de métodos de bottom-up que não conseguem oferecer o melhor controle geométrico. Foi comprovado que a geometria desempenha um papel crítico no comportamento vascular das micropartículas, daí a necessidade de obter portadores não esféricos.

Este projeto propôs utilizar métodos de fabricação top-down de forma a superar essa limitação. Com o objetivo principal de desenhar e fabricar três formas diferentes de microgéis à base de PEG (hastes, estrelas e hexágonos) projetadas para dimensões semelhantes às hemácias. Primeiramente, foram produzidos templates de silício com os padrões fabricados por fotolitografia e erosão seca. Em seguida, estes foram usados para imprimir moldes de polímero de ciclo olefina (COP) por hot embossing. A estes moldes foram depositadas diferentes formulações de PEG (com e sem Hb) por slot die coating. Consecutivamente, estes foram usados em UV-assisted punching para obter as desejadas formas microgéis com o molde cortando mecanicamente as formas pelo hidrogel para o substrato de álcool polivinílico (PVA). Posteriormente os microgéis foram obtidos através da dissolução do PVA em água. Sendo que estes mantiveram os tamanhos desejados com uma razão de aspeto de 3:1, conservando também as formas. No entanto, os desafios permaneceram na obtenção de microgéis individuais após a dissolução. Devido a limitações de espessura durante a deposição que consequentemente afetaram o processo de cortamento mecânico posterior.

Palavras chave: Hemácias, polietilenoglicol (PEG), templates de Silício, moldes de polímero de ciclo olefina (COP), microgéis, slot die coating, UV-assisted punching.

CONTENTS

List of Figures

List of Tables

ACRONYMS

RBC	Red Blood Cell
HMDS	Hexamethyldisilazane
FDTS	Perfluorodecyltrichlorosilane
PEB	Post-exposure bake
MVD	Molecular vapor deposition
CEA	2- Carboxyethyl acrylate
BHF	Buffered hydrogen fluoride
PEG	Poly(ethylene glycol)
PEG MA	Polyethylene diacrylate
PEG DA	Polyethylene glycol monoacrylate
IPA	Isopropanol
PVA	Poly-vinyl alcohol (PVA)
COP	Cyclo olefin polymer
RIE	Reactive Ion Etching
DRIE	Deep Reactive Ion Etching
AOE	Advanced Reactive Etching
SEM	Scanning electron microscope
AFM	Atomic force microscopy
UV	Ultra-violet
CPR	Central point runs

SYMBOLS

mm	Millimeter
cm	Centimenter
m	Meter
nm	Nanometer
µm	Micrometer
mL	Milliliter
µL	Microliter
g	Gram
L	Liter
rpm	Rotations per minute
W	Watt
Sccm	Standard cubic centimeters per minute
kV	Kilovolt
min	Minute
s	Seconds
h	Hours
ppm/K	Parts per million per kelvin
mPa	Millipascal
mN	Millinewton
°C	Degree Celsius

1

INTRODUCTION

1.1 Motivation and objectives

Blood products, specifically red blood cells (RBCs), are a vital necessity in daily clinical practices globally, due to the constant high demand for blood transfusions such as for blood disorders, traumatic injuries, and surgical operations. Yet the response to this need is under permanent and detrimental limitations related to donor-derived blood sources. Limitations such as insufficient availability, short shelf-life, risk of pathogenic contamination, and the need for blood typing and cross-matching [1]. Furthermore, only 7% of donors possesses "universal" O-negative blood, blood-based products have a lifetime of a maximum of 42 days, under refrigerated conditions, or 1 day at room temperature, and they require expensive screening to prevent any disease transmissions [1][2]. Scientific research is pushing in the direction of tackling this large number of challenges, by developing hemoglobin (Hb)-based oxygen carriers (HBOCs) as artificial RBCs. HBOCs are designed to substitute and amplify the functions of endogenous blood components. However, this goal still remains a holy grail, thus the importance of this study.

Currently, microparticles and nanoparticles as encapsulated systems have been revolutionizing the drug delivery field. In this specific case, Hb encapsulation in microparticles would ensure protection from plasma-induced effects, increase the circulation time, and allow sustained availability to cells, tissues, and organs [3]. The aim of this study was to fabricate PEG-based hydrogel microparticles as vehicles of encapsulation, since these are believed to be nonimmunogenic, biocompatible, and biodegradable [4].

The drug delivery field in still mainly focused on spherical carriers made by bottom-up self-assembly, which creates a high demand for further exploration in non-spherical carriers made by different approaches since the geometry of the particles plays a crucial role in their vascular behavior [5]. Additionally, the quality control of the shape and size of non-spherical particles is still a pressing challenge in the industry. Top-down fabrication methods have proven to offer better control over the size and shape of these polymeric carriers, since they start from the material in bulk. This project focused on an extensive and complete study of a series of top-down fabrication methods used to obtain size specific microgels with non-spherical shapes (rods, hexagons, and stars). The goal was, not just, to mimic the endogenous RBCs size features (aspect ratio 4:1), but also, to offer a comprehensive analysis of the microfabrication methods used, as well as a proper monitoring of size and shape through suitable characterization techniques. The exact objectives were to first design these shapes with 10 µm of length and make a periodical array for each pattern. Then use these patterns for photolithography and consequently dry etching processes to fabricate three different Si master templates, with microstructures of ~3 µm in etch depth, resulting in an aspect ratio of ~3:1. Afterwards, use these as mold to imprint the inverted design onto a cyclo olefin (COP) polymer polymer, fabricating stamps through hot embossing.

These stamps would be then coated, by slot die coating, with PEG-based solutions (with and without Hb), and a substrate would be stacked on top. This stack was proposed to be used in the final process, UV-assisted punched to obtain the microgel shapes. In this last process the specific aim was to form the microgels and mechanically punch thought the hydrogel flash layer onto the PVA substrate. Lastly these microgel shapes would be easily harvest by PVA dissolution in water.

1.2 Hb-based O_2 carriers (HBOCs)

RBCs are the most dominant cell type in our body since they are responsible for transporting 98% of all the oxygen (O_2), through a protein called hemoglobin (Hb)[2]. RBCs have the shape of a biconcave discoid with ~8 μm in diameter and ~2 μm in thickness, being highly flexible and viscoelastic to increase their surface area for optimal O_2 diffusion [1]. This high flexibility allows them to also deform and squeeze through smaller capillaries and deliver oxygen to the tissues [6]. Hemoglobin (Hb) is a tetrameric protein consisting of two α and two β-polypeptide chains, where each possesses an iron-containing heme group capable of binding one oxygen molecule (O_2) [6]. It is important to reference that if the tetramer dissociates into dimers and monomers, then this acellular Hb becomes toxic [3]. This is the case because it can permeate in between the endothelial cells lining our blood vessels into the smooth muscle tissue [7][8]. Additionally, free Hb becomes more viscous, and it also affects the osmolarity of blood, thus leading to alteration of blood volumes [9]. Hb also tends to degrade with temperature and in the presence of specific solvents. Therefore, due to these toxic effects semi-synthetic systems called HBOCs started being developed to employ natural Hb either by chemical-modification or by encapsulation, to minimize tetramer dissociation, extravasation, rapid clearance by the kidneys, as well as prolong blood circulation, without compromising the capacity to transport O_2 [3].

The chemical-modification approaches consisted in Hb cross-linking (between different subunits), polymerization (bifunctional cross-linking reagents) and conjugation to biocompatible polymers (e.g., PEG). The encapsulations approaches focused mainly on microparticles and nanoparticles to be used as surrogates. This study focused on an encapsulation approach since with the Hb entrapped within a carrying vessel, it would be easily shielded from direct contact with other blood components and the surrounding tissues [10]. This consequently reduces the Hb viscosity, the colloidal osmotic pressure and the hypertensive responses, as well as the uptake by macrophages. Additionally, although both the chemical-modification and encapsulation enable surface functionalization, only encapsulation allows for incorporation of additional active compounds within the same carrier. However, the disadvantages of this approach is its complexity to produce carriers, due to the broad range of possible structures and materials, which translates in costly processes and difficulties to scale-up with likely batch-to-batch variations. There are also challenges in loading high Hb quantities in comparison to the chemically modified approaches, and the encapsulation itself can compromise the diffusion of O_2 in and out of the carrier[1]. Nevertheless, this approach was still chosen since it comes closer to fully mimic the endogenous RBCs.

Regarding the specific carriers it needs to be understood that the geometry of the carrier plays an important role, since the particle size and shape determines how the body responds, distributes, and eliminates the microparticles[11]. Until now mainly spherical particles have been developed. These particles showed, when intravenously (IV) introduced, shorter circulation times, in comparison to non-spherical particles. Non-spherical particles also proved reduced phagocytosis by exhibiting lowered liver accumulation, thus demonstrating increased accumulation in other organs [5]. Within the developed non-spherical particles, mostly shapes such as elliptical disks[12], nanorods[13], disks and nanoworms[14] have been exploited. This means there is a demand for further research to be pursued for other geometries. This is challenging due to increased

complexity in their fabrication. In this project the aim was to tackle this by designing and fabricating three non-spherical carrier shapes (rods, stars and hexagons) within the same size range.

1.3 Poly(ethylene glycol)-based hydrogels

Hydrogels are three-dimensional (3D) cross-linked polymer networks that have demonstrated great potential for biological and medical applications. Hydrogels are hydrophilic polymers with high resemblance to the microenvironment of several tissues in the human body, thus exhibiting excellent biocompatibility [15].PEG is a linear synthetic polyether that can be prepared using a wide range of sizes and terminal functional groups. It can by synthesized by anionic ring opening polymerization of ethylene oxide with a range of end groups (e.g., methacrylate or diacrylate) attached. Furthermore, PEG is a hydrophilic polymer, that is water soluble, nonimmunogenic, biocompatible, biodegradable and flexible[16]. The stability of polymeric materials depends on factors such as water content, pH, temperature, exposure to UV light or presence of enzymes[17]. In this specific case, PEG-based hydrogels were used for Hb encapsulation since they showed great potential in tissue engineering and drug delivery systems owing to the reasons stated before. The cross-linking happened through free radical polymerization, which used an UV sensitive photoinitiator, two polymeric chains and a crosslinker, that led to a copolymeric hydrogel synthesis. This approach allows for spatial temporal control during the growth of the polymeric chain, as well as exceptional biocompatibility. To elaborate, first the photoinitiator molecules were converted into free radicals upon UV exposure at room temperature. Then these radicals promoted the increase of reactivity between the monomers and the crosslinker, and the resulting electron transfer forms covalent bonds between them and allows for the growth of the polymeric chain. The specific properties of the obtained hydrogel (such as mechanical strength, physical integrity and swellability) are directly dependent on the concentrations used during formulation [18].

1.4 Fabrication Methods

Top-down and bottom-up methods have both been used to fabricate non-spherical particles. Bottom-up fabrication processes assemble materials from atoms or molecules, and have been the main focus in the fabrication of spherical carriers as well as non-spherical [5]. However, in this project the aim is to fabricate three different non-spherical microparticles (rods, stars, and hexagons). For this purpose, top-down fabrication approaches are better suited. This is the case because these approaches start from the bulk material, which can provide better consistency in terms of particle size, shape, and geometry. Additionally, top-down fabrication has been well established for micro-electromechanical systems (MEMS) to fabricate 3D geometries with high precision, and more recently it has also been used in biomedical applications to achieve desired features in carriers[19][20]. In this specific study the top-down fabrication methods used were centered on photolithography, dry etching, slot die coating and imprinting (hot embossing and UV-assisted punching), to obtain the desired shaped hydrogel microparticles. In the following, the basic concepts of these fabrication methods will be briefly introduced.

1.4.1 Photolithography

Photolithography is a method often applied in semiconductor manufacturing of microchips, and it is of a photon-based technique that projects an image of the desired pattern onto a photoresist (PR), coated onto a substrate [21]. It allows for patterns resoltution as low as 10 nm[22]. The photoresists used may be positive or negative. For the positive photoresists the exposed areas are dissolved when developed, and for the negative

photoresist the same happens but to the unexposed regions instead. The pattern resolution in this technique is directly controlled by the light exposure, which depends on the specific light source used. Additionally, this method allows for fast transfer of dense patterns while offering high resolutions at micro and nanoscale.

1.4.2 Dry Etching Techniques

Dry etching consists of the removal of substrate material through etchant gases or plasmas. Dry-etching techniques are devided as physical dry etching (kinetic energy of particle beams), chemical dry etching (chemical reactions between etchant gases), and physical–chemical etching (etchant gases excited by ions). In this project only physical-chemical etching was explored, since this method uses plasma etching which offers the best control over the final features, due to higher process pressures. More specifically it will focus on Advanced Oxide Etch (AOE), for etching SiO_2 and on Advanced Deep Reactive Ion Etching (DRIE) for etching microstructures into Si (CORE process). Both these processes are based on Reactive Ion Etching (RIE). RIE involves an initial introduction of etching gases (such as fluorine and chlorine-based gases) in the etch chamber. The plasma is generated by the ionisation of electrons due to dissociated gas molecules at high voltage. These radicals directed towards the substrate surface where chemical reactions take place, resulting in volatile reaction products that are removed from the etch chamber. [23][24] The first (AOE) was based on Inductively Coupled Plasma (ICP) technology, which consisted of a generation of plasma by a radio frequency (RF) powered magnetic field plasma, with a separate RF generator that directs an electrical field to steer the reactants toward the substrate and obtain a highly anisotropic etch result [25]. This allows for higher plasma densities to be created at a lower pressure, which consequently increases the etch rates and ensures a more anisotropic etch profile. Consequently, it allows deeper etches into materials. However, it is not efficient enough for high aspect-ratio (HAR) anisotropic etching of single-crystal silicon, in comparison to DRIE etching process. A CORE (Clear, Oxidize, Remove, and Etch) etching sequence similar to the SF_6-based Bosch process was run in the DRIE tool. These are cyclic processes consisting of alternating etching and deposition steps, that allows for polymeric films to be deposited onto the Si surface protecting the sidewalls (passivation) and ensuring HAR anisotropic etch in Si. In a CORE process the usual (octafluorocyclobutane) C_4F_8 inhibitor used in a traditional Bosch process is replaced by O_2 oxidation. This replacement is advantageous since the C_4F_8 inhibitor has a long atmospheric lifetime, making it a severe environmental problem, due to its direct contribution for the global warming. Lastly, this etching process ensures a better control over 3D profile at room temperature, as well as enables higher selectivity. [26]

1.4.3 Nanoimprint Lithography (NIL)

NIL is a straightforward mechanical lithography technique that consists in replicating the pattern of a specific embossing master template, by imprinting it into a deformable polymer substrate. The imprinting tool used in this project consists of a closed vacuum chamber, that on the inside has a metal plate on the bottom, which can be heated, and on top has a pressure membrane, that will control the force applied to the materials stacked within this tool during an embossing cycle. This method has demonstrated the ability to replicate with high precision micro and nano-scale features in the templates used [27]. It is a low cost and high reproducible process that can be easily used for mass production. During this project two distinct NIL processes were used in two different fabrication steps. The first is a well-established technique called hot embossing (thermal NIL) which was used to fabricate cyclo olefin polymer (COP) stamps, and the second, is a derived technique called UV-assisted punching (UV-NIL) developed by DTU, used to fabricate the individual PEG microgel shapes on a poly(vinyl alcohol) (PVA) substrate. Thermal NIL focuses on several main operating parameters such as applied pressure, heating temperature, embossing time, and demolding temperature. It runs an embossing cycle

where both the tool and the materials (master and substrate) are heated in the chamber to a temperature between the glass transition temperature (T_g) and the melting temperature (T_m) of the polymer material. At the same time the tool applies an embossing pressure and brings into contact the heated layers (master and substrate), resulting in transfer of the inverted pattern in the master (3D shaped microstructures). Then the temperature lowers to the demolding temperature to ensure the stabilization of the pattern imprinted onto the polymer (microwells). It needs to be noticed that there are differences in the temperature coefficients between the embossing master and the substrate. This could generate unwanted increase of friction forces and shrinkage of the polymeric material during the demolding and the cooling step, respectively. [28] Which can affect not just the replication fidelity of the pattern (deformations), but also, depending on the features of the microstructures patterned into the master (aspect ratio), it can result in significant damage of the microstructures in the Si master. The substrate used in this study was COP, which is a transparent and thermoplastic polymer material, used frequently in replication applications, with low surface energy (hydrophobic), good thermal stability and high tensile strength [29]. The UV-assisted punching is based on the same concept as thermal NIL. However, UV radiation is added during the patterning process, which typically is referred to as UV-NIL. UV assisted punching works at room temperature, and the operating parameters are the applied pressure, the UV dose, and the embossing time. It was chosen for this study since the aim was to encapsulate Hb, and at room temperature, Hb denaturation could be avoided. In figure 1 can be seen an illustration of the different NIL processes explained. An image of an example of NIL tool (imprinter) can be found in appendix A.

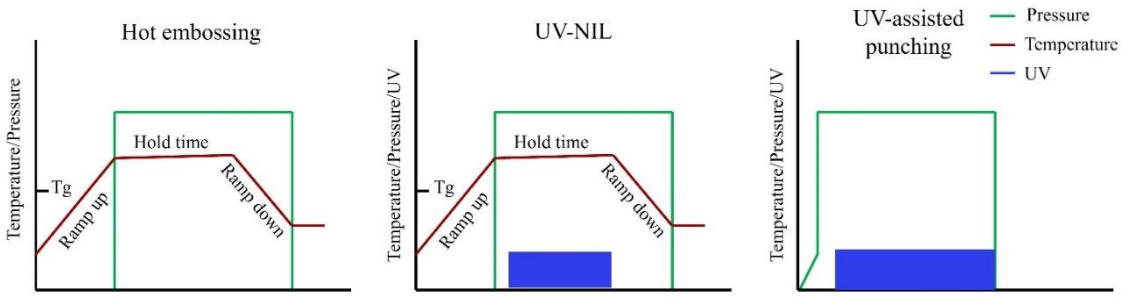

Figure 1 - Illustrations of the different embossing cycles in each NIL process (Hot embossing, UV-NIL, and UV-assisted punching).

This process uses a coated stamp (filled microwells) and a transparent substrate. It aims to cure though UV exposure the coated film (form hydrogel) and mechanically punch though this hydrogel onto the substrate, using the pressure applied during this embossing cycle.[30][31] After substrate demolding from the stamp, this will result in the final microgel shapes imprinted onto the substrate. In figure 2 this process is represented. The mechanical force used in this process is substantially smaller than NIL, since it requires less embossing pressure. This plus the fact that it is at room temperature, ensures a minimization of possible distortions in comparison to the former process.

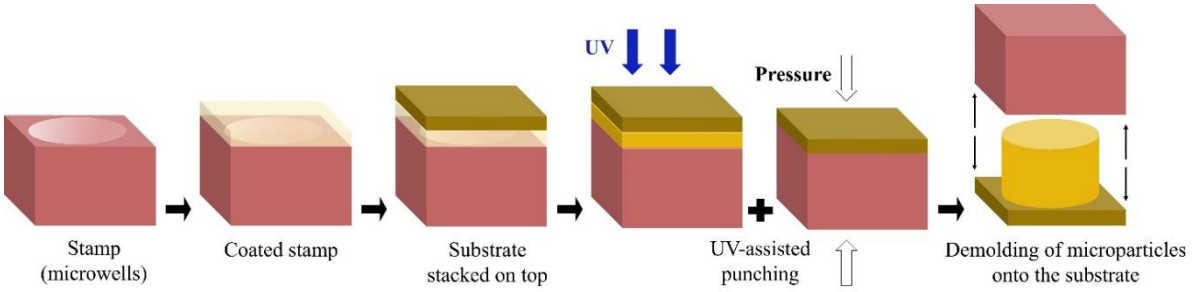

Figure 2 - Illustration of the UV-assisted punching process.

In this study the substrate chosen was PVA which is a synthetic transparent polymer chosen for its highly solubility in water and great mechanical properties [32]. A thin film of the PEG-based hydrogel

formulation was coated onto the stamp, through slot die coating. Additionally, COP was chosen as stamp in this process over the standard Nickel (Ni) stamps used in earlier studies, since the aim was to produce micro-gels which would require further cleaning in the case of using Ni stamps, hence by employing polymeric stamps the process becomes easier and faster. Lastly these challenges regarding the demolding step afterwards are directly depended on the coating and also on the surface energy of the COP stamp, since it can facilitate or compromise the adhesion to the substrate.

1.4.4 Slot die coating

Slot die coating is a polymer deposition process commonly used for the industrial production of thin and uniform films, though a precise coating onto a substrate[33]. When comparing to more traditional deposition methods such as spin-coating, this method offers potential for large scale, and less material waste. It is commonly used to produce dry polymer films, although it can also be used to produce wet films. The film thickness is determined by the major operation parameters such as coating speed, flow rate, coating distance, volume dispensed, coating gap, and vacuum pressure. The slot die coater runs an automatic process and it comprises of a head and a plate, that moves horizontally with a certain coating speed and where vacuum can be applied to the substrate. In addition, the head itself consists of several critical metal components, which are: the two main planes (front and back), that constitute the head, and, inside the head, two metal sheets, a meniscus guide, and the shim. Image of these can be found in appendix A. These are all mounted together by alignment pins and security bolts. The shim is a cut-out section that guides the liquid internally in the direction of this lip. In the front plane, there is also a manifold, which is the liquid distribution chamber with a specific geometry. Lastly this process offers a range of different design considerations for the meniscus guide, the shim and the manifold (shaped area inside the slot die head) which can improve the stability of the meniscus and consequently ensures high coating uniformities [34]. The slot die head is positioned close to the substrate and it is used to dispense the coating on the substrate. A set volume of coating solution is pumped into the head through a connecting syringe. A liquid curtain is formed between the substrate and the lip of the slot die coating head, which results in the coating as the plate moves. The liquid curtain relies on the formation of two stable meniscus that can be seen upstream and downstream of the slot-die lip.[34][35] Method illustrated in figure 3.

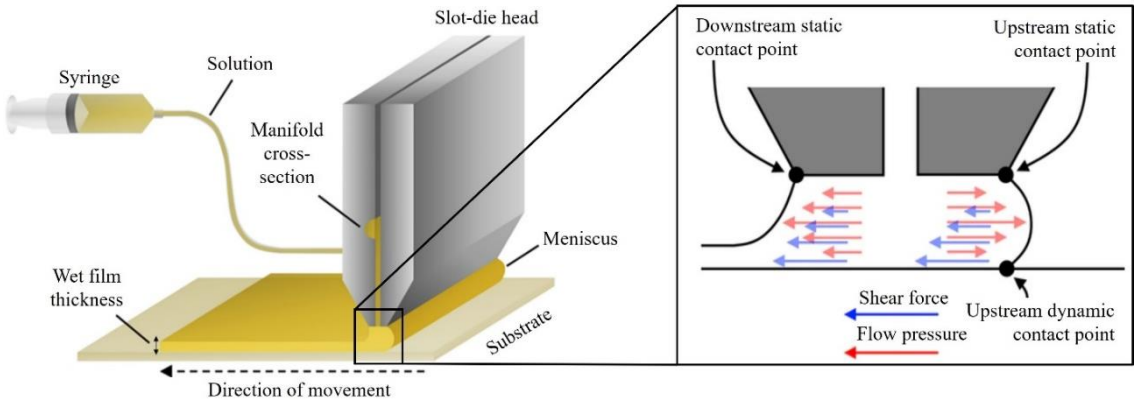

Figure 3 – Illustration of the general mechanism used in a slot die coating process, as well as representation of forces involved in the formation of a steady meniscus (upstream and downstream) between the lip and the substrate. Adapted from: Ossila [34] and Patidar *et al.*, [35].

The challenge in setting the appropriate range of parameters relies on other factors. These include acting competing forces (capillary, viscousness, inertial, gravitational, and shear forces), as well as specific substrate properties (superficial tension). There is a very narrow window of optimal parameters that ensure a high-quality coating with the desired uniform thickness. Outside this window coating defects such as neck-in, rivulets, and air entrainment occur, all resulting in nonuniformities across the substrate.

2

MATERIALS AND METHODS

2.1 Materials

A4 Zeonor (cyclo-olefin polymer, COP) foils (188 µm in thickness) were purchased from Microfluidic Chipshop (Jena, Germany). Polyethylene glycol monoacrylate (PEG MA) (MW=400) was purchased from Dayang chem (Hangzhou) Co. Ltd. (Hangzhouzhejiang, China). Polyethylene diacrylate (PEG DA) (MW=4000) was purchased from Polysciences Inc. (PA, USA). 2- Carboxyethyl acrylate (CEA), Darocur®1173 were purchased from Sigma Aldrich (Søborg, Denmark). Ultrapure water (Milli-Q) was obtained from a Gradient A 10 system, EMD Millipore (USA). Hemoglobin (Hb) (100g/L), previously extracted from bovine blood (Bovine blood with citrate, product no. 77667, obtained from SSI Diagnostica A/S, Hillerød, Denmark). Poly-vinyl alcohol (PVA) sheet (40 µm in thickness), obtained from an unknown source.

2.2 Preparation of PEG-based hydrogel formulations

The PEG-based hydrogel formulation (original formulation) used in this project was prepared with 50% (w/v) materials in milli-Q water, where first 1% (w/v) PEG DA was weighed out, and to this 88% (w/v) PEG MA, 10% (w/v) CEA, and 1% (w/v) Darocur®1173 were added. It was prepared inside a fume-hood, due to involving corrosive and carcinogenic chemicals if inhaled. Then it was vortexed until the PEG DA was dissolved, and the final solution was homogeneous. It was protected from UV light with aluminum (Al) paper and stored at -4°C. In the synthesis PEG MA was used as the main polymer backbone, PEG DA as the cross-linker, CEA as stabilizer (by adding a negative charge to the surface), and Darocur® as photoinitiator. Three other PEG-based formulations were prepared, where Hb was added to the original solution with a range of Hb volumes, 0.1 mL, 0.5 mL, and 1 ml, resulting in the final Hb concentration of 1 g/L, 5 g/L and 10 g/L, respectively, in each solution. In the appendix An image of the four different formulations can be found in appendix B.1, as well as an illustration of the hydrogel formation.

2.3 Design of patterns

The design was made using the CleWin software, and it consisted of a circular periodical array (40mm of radius) for each shape (rod, stars, and hexagons). The dimensions for the rod shape were 10 µm in length with 2.5µm in width, the hexagon shape was regular with six sides made within a circle of 10 µm, as well as the star shape which had six edges. The dimensions were chosen to mimic a size range close to the RBCs (~8 µm in length). The distance between the shapes in the arrays was always made to be ~1µm, but due to differences in shape features the final arrays were not exactly the same regarding the distances between the structures.

2.4 Fabrication methods

The following scheme represents the various process flows of fabrications that will be described in this section.

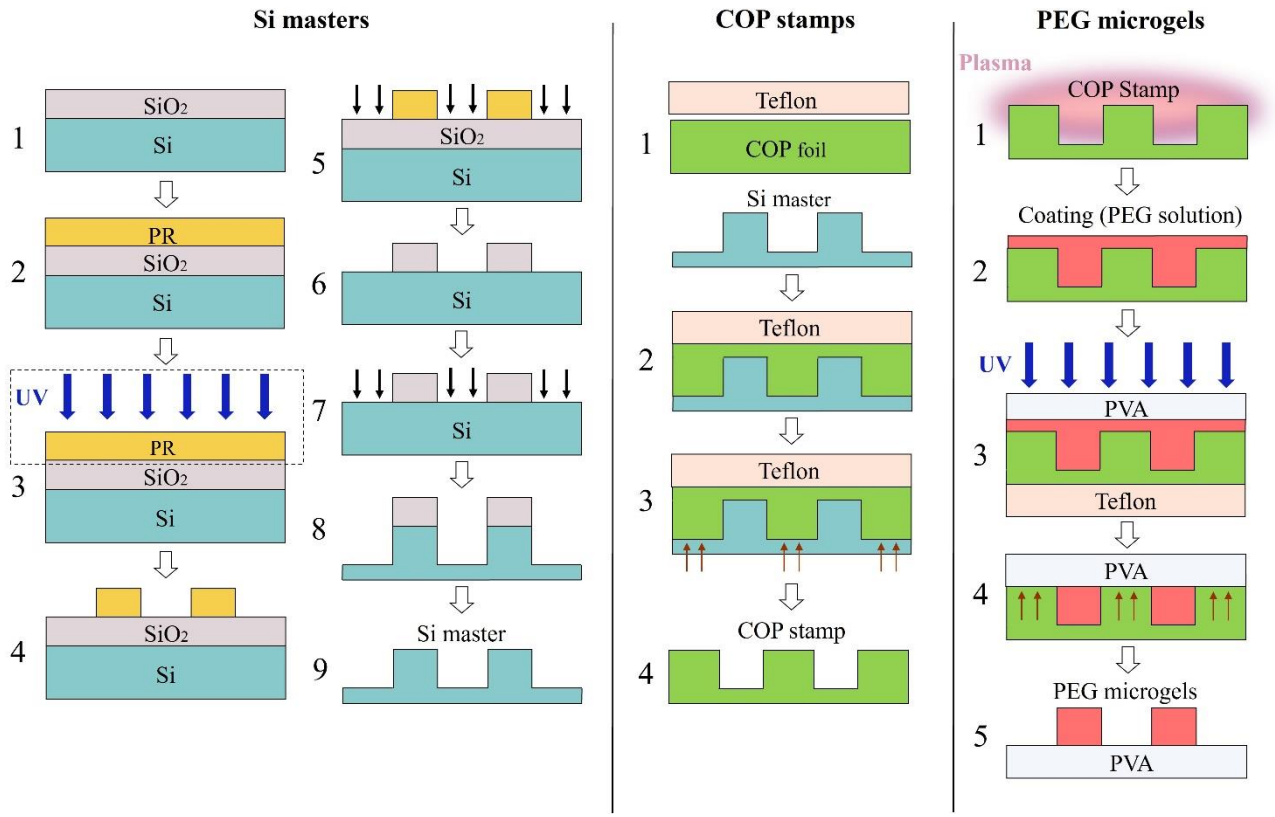

Figure 4 - Schematic of the process flows of the three key fabrications (Si masters, COP stamps, and PEG microgels) used for all three designs (rods, stars, and hexagons). The fabrication of the Si masters involved the following steps: the wet oxidation (1), the UV lithography divided into spin coating (2), UV exposure (3), and development (4), and the dry etching steps divided in SiO_2 etch (5), a strip of the photoresist (6), Si etch (7 and 8), and strip the oxide (9). The COP stamps involved the following: stack of materials (1), hot embossing (2) and demolding (3 and 4). For the PEG microgels, the steps were: plasma treatment of stamp (1), coating of stamp by slot die coating (2), UV-assisted punching (3), and demolding (4 and 5).

2.4.1 Si masters

The masters were fabricated on 4-inch (100mm) single side polished Si (100) wafers. These wafers were wet oxidized in anneal oxide furnace at 1100°C with 60 mins of oxidation and 20 mins of annealing to create a thin film ~500 nm thin film of SiO_2. This layer was used as a mask in the Si etching process.

Next, the wafers were coated with a positive photoresist (AZ® MIR 701) using a Gamma 2M spin coater (Süss MicroTec, Germany). A standard automatic recipe was used to obtain a final thickness of 1.5 µm, that included an initial HMDS priming process of 1 min. This recipe coated 3 ml at 800 rpm, with a spin-off speed of 4600 rpm for 30 s, and a soft baking at 90°C for 90 s.The pattern was transferred into the photoresist with a maskless aligner (MLA 150, Heidelberg Instruments) that exposed the inverted design (gaps between the shapes in the arrays) with UV-light (λ=405 nm), in quality mode with a defocus of -1 and a dose of 180 mJ/cm^2 for all the three patterns. The photoresist was then developed using an AZ 726 MIF developer in a Gamma 2M developer (Süss MicroTec, Germany). A standard recipe for this photoresist thickness, with 2 s

pre-wet at 1200 rpm, puddle dispense of 11 ml at 30 rpm for 7 s, and a spin-off at 4000 rpm for 3 s, that also included an initial PEB at 110°C for 60 s was used for this development.

Next the SiO_2 was etched using this photoresist pattern as the mask in an Advanced Oxide Etcher, (STS MESC Multiples, UK) a standard recipe used for 2 min 30 s with an etch rate of 200 nm/min, 174 sccm He, 4 sccm H_2 and 5 sccm C_4F_8 at a chamber pressure of 4 mTorr, platen temperature of 0°C, platen power of 200 W and a coil power of 1300 W. After this initial etch the wafer was stripped of the photoresist mask and cleaned through plasma ashing for 40 mins in a Semi Auto Plasma Processor 300 (TePla, Germany). With an O_2 flow of 400 ml/min, an N_2 flow of 70 ml/min, at a power of 1000 W.

An Advanced Deep Reactive Ion Etching, (SPTS LPX Pegasus, UK) was used. This process was optimized to obtain the desired depth of ~3µm. The ramping time of the final etch step as well as the number of cycles were optimized, resulting in different central point runs (CPRs). All the other parameters were already fairly established for Si etching and therefore no optimization was required. These can be found in appendix B.2, along with the detailed parameters for the different central point runs (CPRs). The oxide mask was then striped by immersing the wafers in a buffered hydrogen fluoride (BHF) bath for 20 min.

Finally, the masters were coated with an antistiction layer of perfluorodecyltrichlorosilane (FDTS) by molecular vapor deposition (MVD100, Applied Microstructures Inc., USA). The specific recipe parameters can be found in appendix B.2.

2.4.2 COP stamps

4-inch wafer-sized foils were cut out from a COP steet. These were cleaned with isopropanol (IPA) and water to remove any contaminants prior to processing. Next, the inverse topographies of the Si masters were transferred into these COP foils by hot embossing (CNI 2.0, NIL technology, Denmark), resulting in microwells. An aligned stack was prepared inside the imprinter, comprising of the Si master, COP foil, and Teflon foil to compensate for pressure non-uniformities during the process. The embossing cycle was run under a vacuum of 25 bars at an embossing pressure of 6 bars, embossing temperature of 180°C, embossing time of 10 mins, and release temperature of 40°C. After processing, the COP stamps were manually demolded form the Si master. Lastly the COP stamps were plasma treated with O_2 gas in an electronic Diener low pressure plasma system (ATTO, Germany) at a pressure of 0.2 mPa for 2-3 s, to increase their surface energy, which would be crucial for the next steps.

2.4.3 Microgel shapes

The coating of PEG-based formulations, previously prepared, onto the microwells in the COP stamps was done by a slot die coater (FOM vectorSC, FOM technologies, Denmark). A syringe with an internal diameter of 22 mm was used to pump the solution to the slot die coater's head with a meniscus guide of 50 mm width. Due to the narrow window of proper operating parameters, the volume dispensed, and gap height had to be optimized to obtain the desired film thickness of ~ 3 µm. Other parameters stayed constant including a coating speed of 0.5 m/s, and the coating distance of 170 mm. Two main parameters were varied, the volume of solution dispensed (100(10) 40 µL, and 35 µL) and gap coating distance (kept constant at 0.36 mm for volumes until 50 µl, and at 0.24 mm for 40µL and 35µl). With 35uL and 0.24 mm as the final parameters for the formulation with no Hb and with an Hb concentration of 1g/L. The other two concentrations of Hb, 5g/L and 10g/L, used the same gap but the volume was increased to 40 µL, due to the increase in fluid viscosity.

UV-assisted punching performed with UV nanoimprint lithography tool (CNI 3.0, NIL technology ApS, Denmark), at a wavelength of 365 nm and an intensity of 100 mW/cm^2. An aligned stack consisting of a foil

of Teflon, a coated COP stamp and a PVA foil as substrate, was assembled in the imprinter. This technique was directly dependent on the efficiency of the hydrogel coating process, as well as on variations regarding the features in each pattern (different shapes). Thus, it required further optimization to form the hydrogels and obtain full mechanical punching. In the appendix B.3 it can be found a detailed explanation with the parameters used in this process. After the embossing cycle the PVA with the PEG microgel shapes on top was demolded from the stamp and dissolved in water in 5 mL to harvest the microgel shapes. Next, a filtration with a grade of 1 with a pore size of 11 µm and 30 mm diameter was performed. This was done to ensure that only individual microgel shapes where finally obtained. The resulting suspension obtained was centrifugated for 5 mins at 13400 rpm. This resulted in a small pellet with the microgel shapes. Images of these last steps can be seen in the appendix B.4. The supernatant was removed and pellet was resuspended in 0.5 mL of milli-Q water to achieve a high concentration microgel shape suspension.

2.5 Characterization methods

An optical microscope (Nikon ELIPSE L200N 4, Japan) was used to inspect the features after the steps in the fabrication of the Si masters and of the COP stamps. It was also used to inspect how the masters looked after hot embossing and, in a few tests, to characterize the stamps immediately after coating with hydrogel solution. Images were collected at a 100× amplification, and image processing including measurements of features on the masters and in the stamps were performed using the ImageJ. Optical microscope (Olympus Inverted IX83 microscope, Japan) was used to observe the harvested microgel shapes from the small pellet in solution, through a bright field mode and 60× oil-immersion objective.

Characterization by scanning electron microscopy (SEM) with a Zeiss Supra 40 VP SEM (Zeiss, Germany) was used to inspect and analyse surface morphology of the microstructures on the Si masters, the microwells in the COP stamps and the PEG microgels shapes on the PVA substrate. It was also used, while optimizing the Si etching process, employing manually diced cross-sections (~0.5cm × 0.5cm). The imaging of the COP stamps and the microgels shapes on the PVA, required the deposition of a gold (Au) coating, due to the surface charging owing to the transparency of these materials. This coating was deposited using a sputter coater (Cressington 208 HR sputter coater with gold target, UK) for 10 s (rate of ~ 0.7 nm/s). All the micrographs were collected at 10 kV with the immersion lens (InLens) in high vacuum mode. In addition, a SEM Tabletop (Hitachi TM3030 Plus tabletop SEM, Germany) was used for the same purpose, however, only for inspection of small samples of microgels shapes on the PVA, mounted in a 45° holder. All micrographs were collected at a 15 kV voltage using a combination of the SE and backscattered electron (BSE) detection modes.

Characterization by atomic force microscopy (AFM) with an AFM Dimension Icon PT (Veeco Instruments Inc., USA) was used to measure the height of the microstructures in the Si masters and the microgel shapes on the PVA, and the depth of the imprinted microwells in COP stamps. AFM scans were performed in the tapping mode for 6 µm deep trenches using a special probe (FIB6-400A). The data from the AFM was further analyzed with Gwyddion, where 3D images of the different structures were created along with plots corresponding to the structural height profiles. Lastly, due to equipment challenges the height characterization of the star microgel shapes had to be made using an optical profilometer (Olympus LEXT, Japan) as an alternative.

3

RESULTS AND DISCUSSION

This chapter discusses the results obtained during all the fabrication steps and respective characterizations with the final aim of achieving microgel shapes. Furthermore, detailed process optimizations of a few methods, where a range of parameters were varied and studied in order to obtain the best possible results are also described. The challenges faced during the various processes, the cause and consequent potential solutions to overcome them are also discussed.

3.1 Si Masters

3.1.1 UV lithography

Development of the intended design patterns resulted in three different photoresist masks with features in rod, star and hexagon shape. These photoresist masks were used for the following etching processes. Figure 5 shows the various patterns in the photoresist and the shape specific features of the design. The masks were inspected by optical microscopy to evaluate the quality of the UV exposure in the lithography process, through measurements of the feature dimensions. After development, for all patterns measurements were made of the different feature dimensions including length, width, and distance between the structures. These can be found in appendix C. The length measurements are described in table 1, as these were used as the main focus for resolution analyses and comparison between patterns.

Overall, it was possible to obtain high resolution using the AZ® MIR 701 photoresist with the specific optimal dose and defocus as UV exposure parameters. However, it was concluded that the resolution differs from design to design. For instance, by comparing the length of the shapes in the designs, rods, stars and hexagons, in figure 5a, to the measurements of length in table 1, it was observed that the resolution decreases from, hexagons to rods and then to stars.

Table 1 - Average measurements of the lengths across the wafer for each pattern in the Si wafers after development.

Shapes	**Rods**	**Hexagons**	**Stars**
Length (µm)	9.95 ± 0,05	9.83 ± 0,08	9.43 ± 0,07

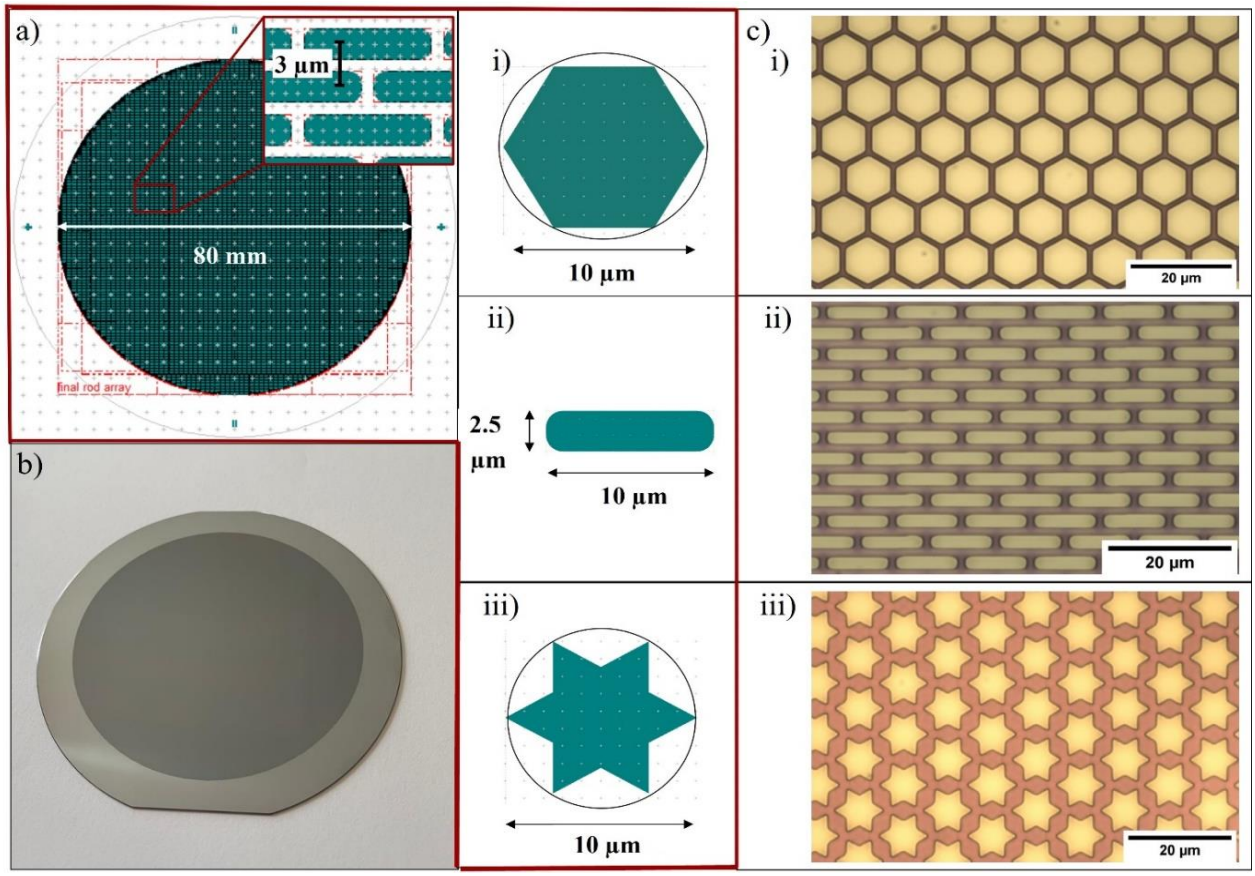

Figure 5 - Si masters design and photolithographic patterns. With: a) a circular array design made in CleWin along with the design of each shape, hexagons, rods, and stars, respectively presented in i), ii), and iii); b) a Si wafer with features in the micron scale; c) the different obtained patterns for each shape in i), ii) and iii)..

These resolution discrepancies may be due to photolithography parameters and the photoresist itself. The exposure during photolithography is dependent on the laser diode, light source, which emits the previous described dose at a given defocus. The defocus allows to compensate for any offsets in the exposure optimizing the pattern exposed quality in different resists and thicknesses. These parameters were optimized for the features for each pattern with an initial dose study which included defocus exposure tests.

The observed resolution discrepancies for the different patterns alternatively may be due to limitations with the patterned shapes in this resist. The key parameter influencing the final shape and size of the feature in respect to the photoresist is the crosslinking quality and uniformity across the shape at nanoscale[36]. The crosslinking during is dependent on the average number of carbon double-bond neighbours available for crosslinking. In this specific case the crosslinking happens in the spin coating process where the resulting layer of the positive photoresist becomes insoluble. Then the areas exposed to the UV are partially decomposed by weakening the crosslinking of these carbon double-bonds. This partial decomposition is fully finalized after development, and it may result in "blurriness" close to the limits of the shapes (crosslinked photoresist). This since the bonds at the boundaries of these shapes, specially at nanoscale, were weaker at the edges in comparison to the middle.

Furthermore, both the stars and hexagons shapes possessed sharp edges, forming acute and obtuse angles, respectively. In addition, in the current designs, it must be taken in consideration that for each of the patterns the distance between neighbouring shapes was ~1µm. This distance between shapes at the limit of microscale, may compromise shape retention owing to the fact that the decomposition of the bonds needs to be increasingly precise for smaller features. Although the AZ® MIR 701 is a well-established photoresist at microscale resolution, it still can possess some limitations for shape retention in the nanoscale. This explains why both the stars and hexagons shapes lose their sharpness and tend to look roundish at the edges, in

comparison to the rods. Nevertheless, there are a few approaches to overcome these shortcomings, such as tone inversion, design inversion, and the design of connecting sacrificial features, which may increase shape retention. Lastly, it needs to be understood that it was hypothesized that the smallest the pitch between final microgel shapes the better would be the mechanical punching, upon UV-assisted punching. Thus, the importance of making the shapes in the designs the closest possible.

3.1.2 Dry etching

The patterns on each Si master served as masks for SiO_2 etch. The resulting pattern in the oxide after the SiO_2 etch was employed as a mask for the final etch in Si. In this section, the results will firstly be focused on inspecting the cross-section SEM micrographs related to the etch processes. Then on the final surface morphology and etch depth analysis of the final Si microstructures.

Any vertical measurements based on the cross-section SEM images were adjusted to 1/sin70° since the micrographs were collected with a tilt of 20°.

3.1.2.1 SiO_2 etch

By observing the cross-section SEM micrograph (figure 6 a) it can be seen that the etch depth was as expected and that the entire oxide thickness was etched with no signs of Si being etched. The process thus demonstrated good selectivity. However, the sidewalls had a roughness, due to pattern transfer of the sidewall defects of the photoresist mask. Additionally, less dimensional control was anticipated in this etch process due to the lack of passivation as it was continuous process.

However, this defect translation observed from the photoresist to the SiO_2 mask becomes insignificant in the next Si etch step. This initial defect was considered inconsequential as the oxide is removed before stamp fabrication in the following steps. Additionally, the photoresist mask tends to be etched as well with high-density plasma during the etch process of SiO_2.Thus the resulting oxide mask no longer possesses the exact dimensions of the original photoresist mask. This is the main reason why the Si etch was performed with an oxide mask instead of just the initial photoresist mask. Hence, if the photoresist is not stripped away before the Si etch, these defects become even clearer, as the etch progresses as seen in figure 6 b.

3.1.2.2 Optimizing the Si etch process

It was desirable that the sidewalls of the structures in the Si master were smooth and with minimal tapering to obtain the best final microgel shapes. This was hypothesized to improve the mechanical punching in the UV-assisted punching process. Regarding the hot embossing process, the smoothest the sidewalls the easier the demolding step, along with a positive tapering of these microstructures. However, the target was to improve the last method of fabrication, UV-assisted punching, due to employing greater challenges in optimization. Furthermore, a specific Si etch depth of ~3µm was desired for all the masters to obtain a final aspect ratio of 3:1, so as to resemble the aspect ratio of the RBCs (4:1).

To fulfil these preconditions, the Si etch was performed by a CORE sequence process. This allowed for excellent anisotropic etch features with sidewall smoothness and minimal isotropic etching. Nevertheless, this process still needed to be optimized to achieve the required etch depth. The optimizations were made on the wafer patterned with rods. Thus, it is relevant to note that since each shape corresponds to a different array, the final etching results will differ slightly according to each pattern. This optimization consisted of varying the ramping time of the final etch step and the number of cycles that were run to obtain the desired depth, as previously explained.

In the first CPR1 the etch depth was lower than the target (1.01 ± 0.02 µm) (figure 6 b). Therefore, in the next recipe, CPR2, the number of cycles was increased, from 25 to 61, while the ramp was kept the same

at 0-15s. As expected, the resulting depth was larger (5.48 ± 0.05 µm) but still not optimal, (figure 6 c) Then for CPR3 the number of cycles and the ramping time were decreased to 52 and 0-8s, respectively. The measured depth in this cycle was the closest to the target (3.06 ± 0.01 µm)(figure 6 d). However, the sidewalls had a slight negative slope, thus further optimizations were conducted. These etching recipes were being tested on small samples of 0.5x0.5 cm that were diced prior to the etch. The results thus were not representative of an entire etch behaviour across a full wafer. This was due to loading effects which will be further discussed in 3.1.2.1. Thus, in CPR4 an entire Si wafer was etched with a further reduction in the ramping time to 0-2s and a slightly increase in the number of cycles to 54. The depth measurements from cross-section samples from the middle of this wafer in comparison to samples closer to the edge showed clear differences related to the loading effects. The trenches in the middle of the wafer had a greater depth (3.62 ± 0.01 µm) than closer to the edges (3.19 ± 0.02 µm) (figure 6 e). Nevertheless, both depths were larger than 3µm. Thus, the recipe was optimized again. In CPR5, no ramping and only a 15 s etch with 54 cycles was performed (figure 6 f) This last optimal recipe resulted in a lower depth in the middle of the wafer (2.61 ± 0.01 µm). Nonetheless, the sidewalls slope was smaller than with any other recipe, and as previously observed that the depth variation across a wafer a feature of the loading, these parameters were considered to be the final optimal ones.

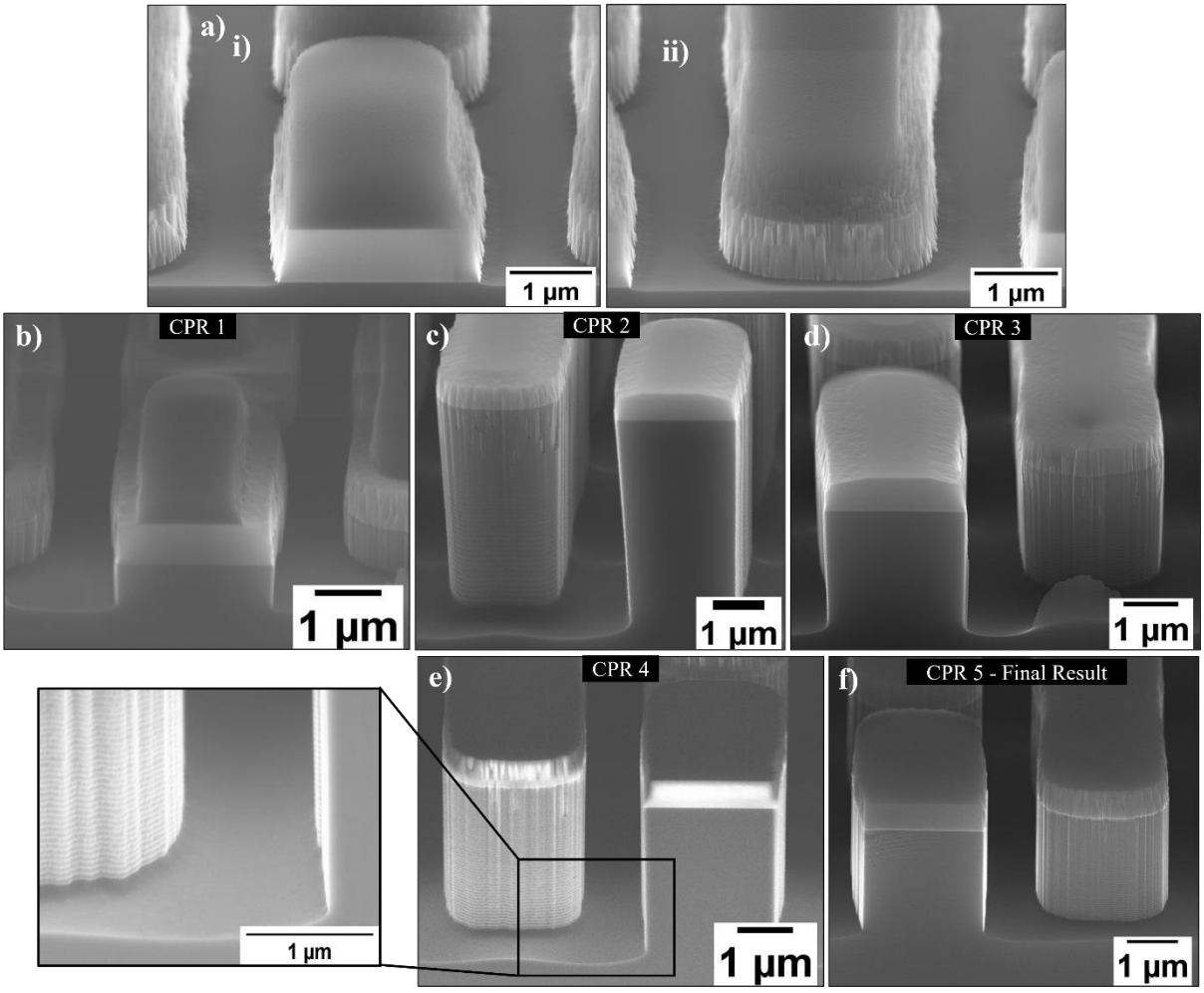

Figure 6 - SEM cross-section inspections showing the results of the Si etch optimization recipes (CPRs) that varied the number of cycles (#) and the ramping etch time (Ra). Where a) is the sample with only the SiO_2 etched, through a still present, photoresist mask, with the cross-section view i) and the sidewall surface view ii). CPR1 run #25 with a Ra of 0-15s in the virgin sample (b), CPR2 run #61 with a Ra of 0-15s (c), CPR3 run #52 with a Ra of 0-8s (d), CPR4 run #54 with a Ra of 0-2s (e), and lastly, the final optimal result CPR5 run #54 with a no Ra with an etch step of 15s (f).

Additionally, from the SEM micrographs above can also be noted that the sidewalls showed visible "scallops", which were expected due to the discontinuous nature of process including passivation.

Furthermore, a few sidewall defects from the pattern transfer of the SiO_2 mask could also be observed closer to the limit with the oxide layer. These decrease as the etch gets deeper, which was also expected due do to passivation steps in the CORE process (oxidation). This is clear to see by observing figure 6 b. To improve the pattern transfer from the photoresist mask to the oxide layer the thickness of this layer could have been decreased, since with a shorter etch process the lateral etch would be minimized. Thus, subsequently improving dimensional control for the Si etch process. Knowing that the DRIE process offers high mask selectivity, reducing the oxide thickness required no compromise.

3.1.2.1 Final Si masters

It is important to also elaborate on the differences in final etch features by comparing characterization results from surface morphology, figure 7, etch depth, and final measured length of the microstructures, table 2, for each Si master fabricated. It is crucial to understand that pattern density effects need to be considered, since etch rates are directly dependent on layout differences.

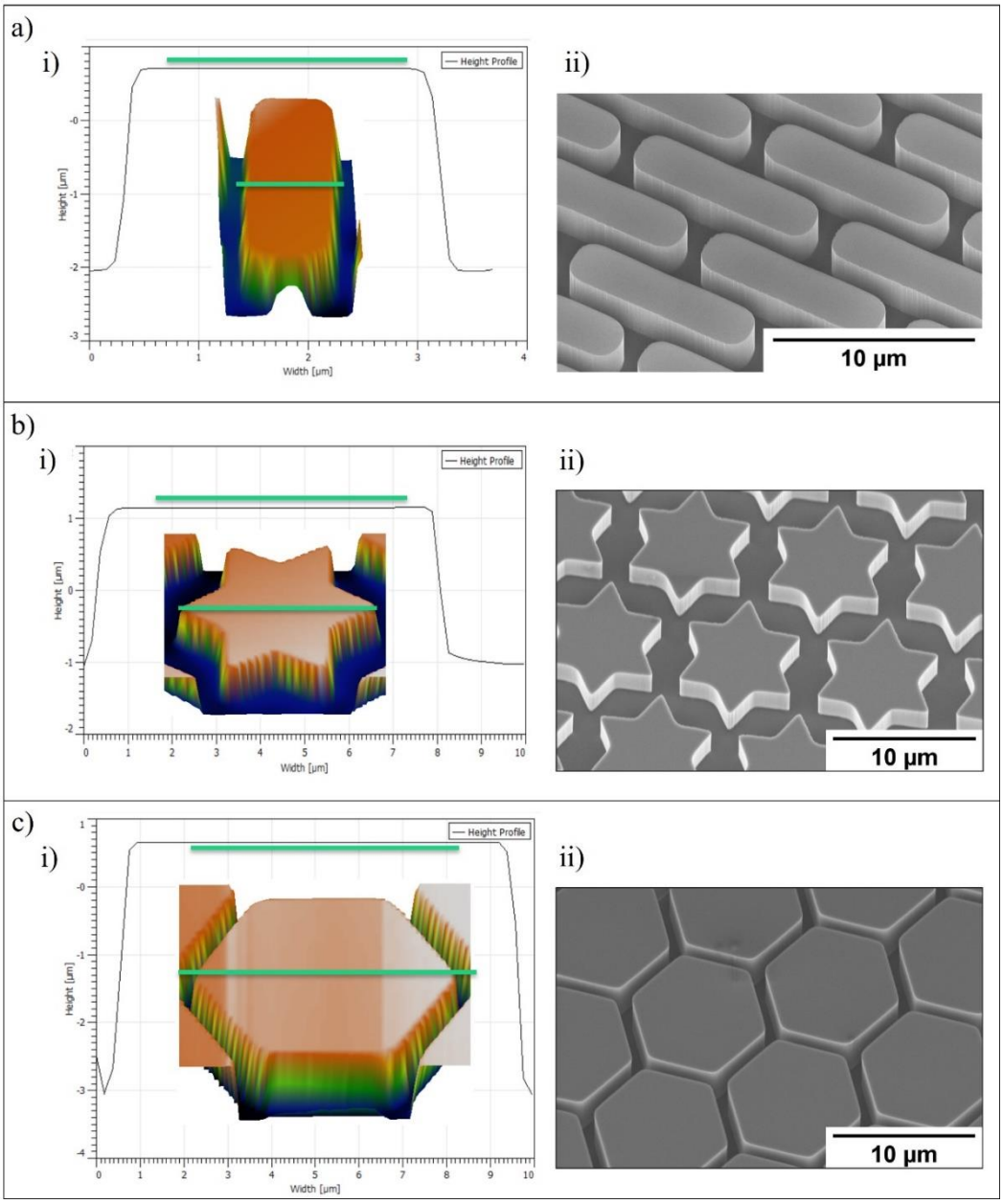

Figure 7 - Si masters topography inspection for all patterns with different shapes, rods (a), stars(b), and hexagons (c). More specifically, 3D topographies of each Si-shaped microstructure within the corresponding height profile plot (i) and SEM inspection of the final etched patterns into the Si substrate (ii).

Table 2 - Average heights and lengths measurements across the wafer of each shaped microstructure in the final Si masters.

Microstructures	Rods	Hexagons	Stars
Height (µm)	2.66 ± 0.18	3.70 ± 0.03	2.48 ± 0.07
Length (µm)	9.87 ± 0.06	9.76 ± 0.08	9.35 ± 0.08

The etch uniformity was defined as the equal etch rate across the wafer, which is directly dependent on the loading effect. The loading effect is the phenomenon in which the etch rate changes depending on the amount of the substrate (Si) area being etched (unmasked area). It is known that for a larger unmasked area the etch rate becomes slower than in comparison to an inferior unmasked area in a pattern, which is affected by the density of the pattern.

For instance, in this specific study, it was possible to conclude that the Si master with hexagons had the narrowest trenches among the three and therefore the densest pattern. In contrast the Si master with stars presents the most unmasked area. Knowing that the process recipe is the same, the gas flow that these wafers will be exposed to is also the same, which would ultimately result in different etch rates. The highest rate corresponding to the master with least unmasked area (hexagons) and the lowest rate corresponding to the master with the least masked area (stars). This explains the different depth measurements for individual microstructures.

These differences could only be mitigated if recipes had been optimized according to the different feature shape. For example, if the pressure had been decreased during the process of the hexagons pattern, or the gas flow had been increased in the stars pattern process.

Additionally, this effect can also be observed on a macroscale level across the entire wafer. In this case, it effects all the patterns the same way and differences are justified as described in section x. The etch depth closer to the middle of the substrate was larger due to the increased load of microstructures, so less unmasked Si area. In contrast, the opposite was measured closer to the edges of the substrate, since it had a reduced load of microstructures, so more unmasked Si area. This occurs due to the depletion of reactants at the etched features, and it can be mitigated by reducing the rate of etching. [24]

Lastly, from the length measurements of these final microstructures in comparison to the ones made for the photoresist mask, in section 3.1.1, along with the final height determinations, it can be concluded good overall dimensional control. Hence, the aspect ratios of these final shaped microstructures were 3:1, as desired.

3.2 COP Stamps

3.2.1 Hot embossing

The COP stamps were characterized for dimensions with optical microscopy, figure 8, and depth with AFM. The surface morphology was characterized through SEM inspections. As before, for the Si masters the full measurements of the dimensions are presented in appendix C. Here the length measurements are presented in table 3, for comparison to the previous measurements of the Si microstructures. This comparison will provide an analysis of fidelity of replication of the patterns imprinted from the Si masters.

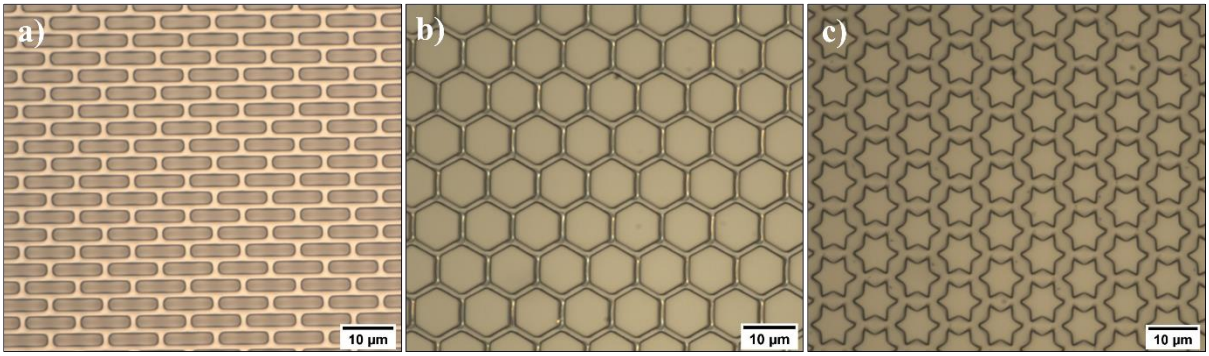

Figure 8 – Inspection through optical microscope of the different imprinted pattern into the COP foils by hot embossing.

Overall, by comparing these measurements, it can be concluded that these resulting microwells possessed length slightly inferior to the initial lengths in the microstructures on the Si maters. However, this was expected as after the completed cooling of the polymer this tends to experience the effect of shrinkage.

Table 3 - Average length measurements of each shape in the COP stamps.

Microwells	**Rods**	**Hexagons**	**Stars**
Length (µm)	9.66 ± 0.08	9.43 ± 0.12	8.77 ± 0.12

In a typical hot embossing cycle, every layer in the stack is exposed to the same temperatures (embossing and ramping temperatures), as explained before in section 1.4.3. Si does not possess a Tg, only the polymer does (COP). Above Tg COP reflows easily filling all the voids in the Si master. Bellow Tg is when it starts the cooling process, shrinking, however it can still reflow if the pressure is maintained.

Thus, near the Tg both parts are in spatial equilibrium, then again, during the cooling the polymer sets and tends to shrink to a greater extent than the Si master. There is a difference in the coefficient of thermal expansion between the Si master (5 ppm/K) and the COP (70 ppm/K) , which justifies these changes in behaviour at the same temperature[37].

With the analysis of the next height profile plots and 3D topographies of each imprinted microwell, it becomes clear that there are some artifacts and deformations in the surface walls of the microwells for the stars and the hexagons wells, figure 9. This implies that for these two shapes either the polymer was not completely yet set, dembossing temperature was not optimal, or it suffered greater stresses upon demolding of the master. Since in rods shapes cannot be observed any deformations and knowing that all the patterns were subjected to the same parameters, it is possible to discard the first option. Concluding that the polymer had an optimal dembossing temperature that allowed it to set properly. This means that the reason must rely on frictional forces employed upon demolding due to the specific geometry of these other Si microstructures (stars and hexagons). These Si microstructures have sharper edges in comparison to the rods, implicating a greater difficulty in achieving a smooth demolding. Although the polymer is already set, his toughness cannot compare to Si, so it results in polymeric deformations seen as roughness at the surface. Nevertheless, this was not too significant, since besides that, the rest of the surfaces (bottom and sidewalls) were smooth and uniform demonstrating a generally saucerful demolding step.

Additionally, depth measurements of these microwells were also made, table 4.

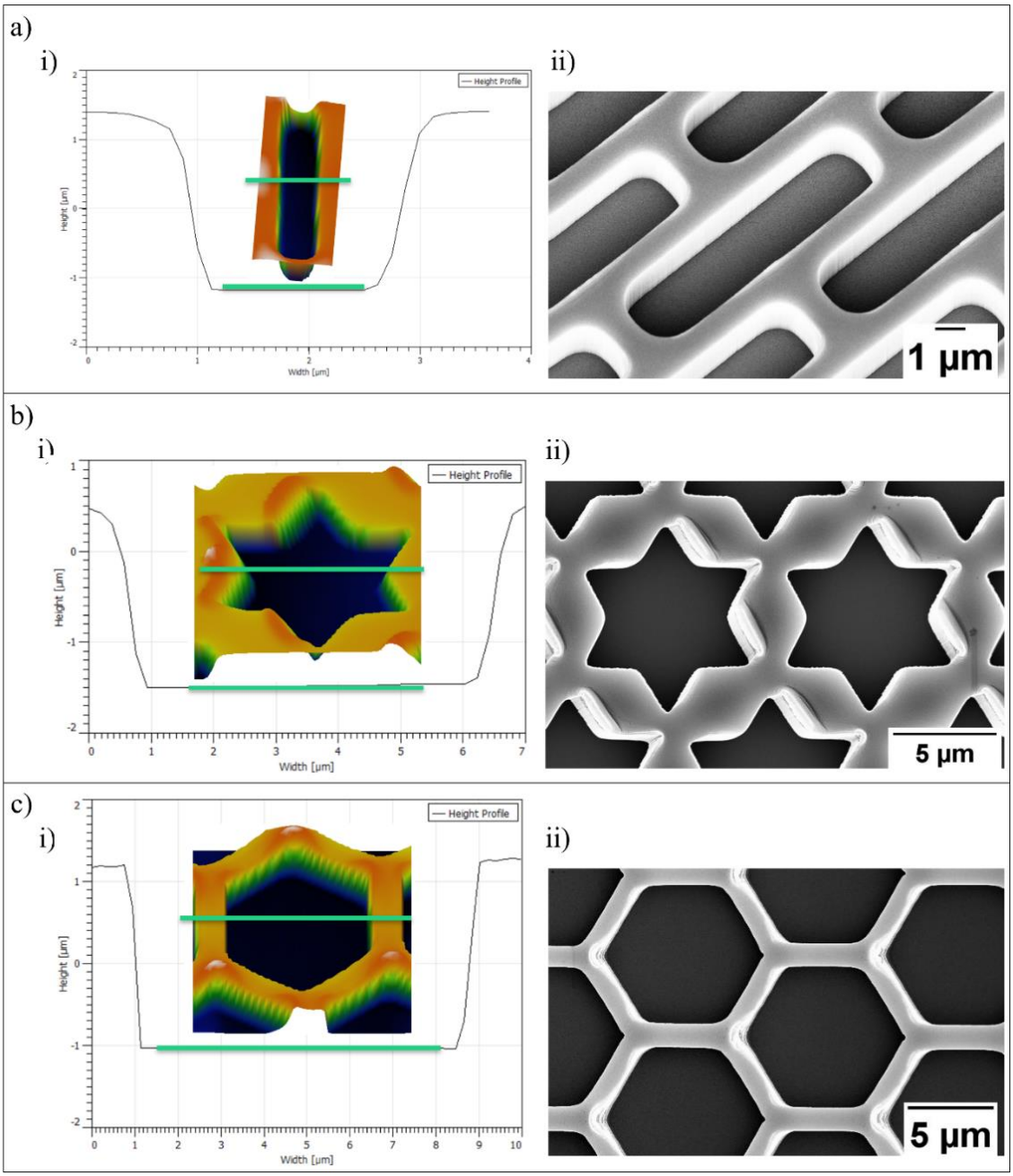

Figure 9 – COP stamps topography inspection for all patterns with different shapes, rods (a), stars(b), and hexagons (c). More specifically, 3D images of each Si-shaped microwell within the corresponding height profile plot (i) and SEM inspection of the final imprinted microwells into the COP foil (ii).

Table 4 - Average depth measurements of each shaped microwell in the COP stamps.

Microwells	**Rods**	**Hexagons**	**Stars**
Depth (µm)	2.44 ± 0.24	3.46 ± 0.31	2.38 ± 0.19

These final depth measurements showed barely any variations from the known height of the microstructures in the Si masters used to imprint. Additionally, these differences as well as the respective higher deviations errors for each measurement, were believed to be a result of these nonuniform deformations observed at the top of the walls of the shaped wells.

Overall, it is possible to also conclude good fidelity of replication of the Si shaped microstructures, which consequently means that the pressure and the time applied during the imprinting process were

appropriate for these patterns. It can also be concluded that the aspect ratio established at the begin in the Si masters remains proportionally the same in all patterns in the COP stamps.

Regarding the Si masters durability these were inspected in the optical microscope, between running imprinting processes, and demonstrated only some remaining polymer in the edges of the arrays. This was not significant to affect the next imprintings, since with the rise of temperature the polymer would reflow again. Additionally, this process showed high reproducibility owning to the Si master durability as well as fidelity of fabrication from stamp to stamp after several repeated embossing cycles using the same master. Lastly, good uniformity of the imprinting across the entire stamp, was also observed through optical microscopy inspection,

3.3 Hydrogel microparticles

3.3.1 Optimizing the slot die coating process

Regarding the optimization of this method, it is important to know the main goal was to achieve a very thin wet film on top of the COP stamps that would be thick enough to fill the microwells. While being thin enough that on top of the filled wells it could form a thin film, of ideally less than 1 μm. Furthermore, this thin film on top was to act as a bonding layer between the microgels shapes and the PVA stacked on top after the coating. Then at the time of UV-assisted punching process, which was the next step to obtain the final microgel shapes, this layer would be mechanically punched, allowing to obtain individual microgels shapes after PVA dissolution. It is detrimental to understand that the coating process and the UV-assisted process were directly correlated and so during this part of the discussion it will be considered as such.

With that said this process demanded a final coating thickness of approximately 3,5 μm. Nonetheless, there was not any approach of determining the specific final coating thickness for such thin wet films in this process. Only after the UV-assisted punching process it was possible to examine this thickness by inspecting the microgel shapes on the PVA substrate. This allowed to verify the existence and approximate thickness of any connecting hydrogel layer between and underneath the microgels shapes, flash layer.

However, there are many aspects related to the COP stamp that need to be mentioned and understood since they can define the efficiency of these two processes. Starting with the fact that the COP stamps had the same area as the original circular layout design with a diameter of 80 mm, as it can be broadly seen in figure 10 c. Still this area could not be fully coated since the meniscus guide only had a length of 50 mm, as it can be seen in figure 10 a, which limited the final yield of microparticles achieved.

Besides, if multiple coatings were performed, it would negatively affect the final thickness due to possible overlaps of coating layers. For that reason, a single layer of coating was performed. The extra substrate area revealed useful in the sense that it allowed spatial advantage during the stacking of the PVA substrate since the liquid could be pushed to the uncoated area and the thickness further improved.

Additionally, the COP stamp was required to be exposed to O_2 plasma treatment to increase the surface energy and consequently allowing for uniform coating (figure 10 b). Otherwise, the liquid would dewett the surface and retract (figure 10 c).

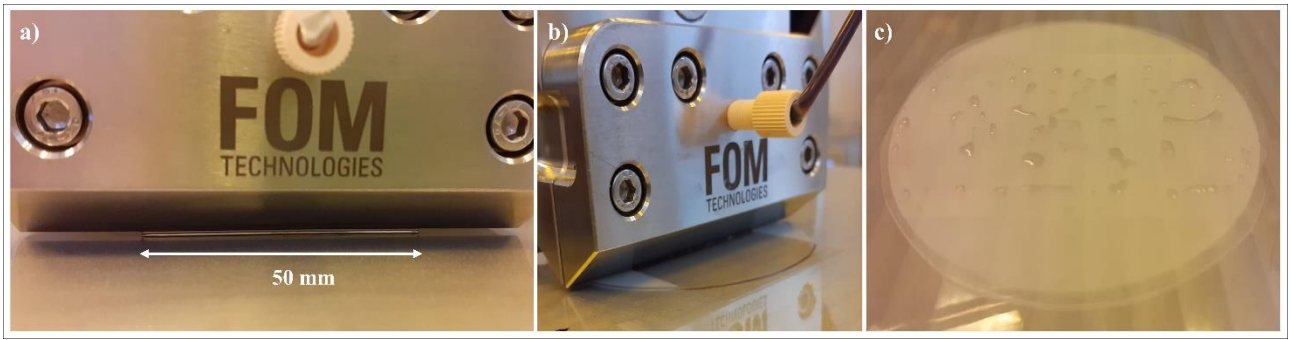

Figure 10 - Coating process of the COP stamps with PEG-based hydrogel formulations. (a) slot die coaters lip where the meniscus guide is seen with a width of 50 mm. The other two images, (b) and (c), represent, respectively, a coating process in a COP stamp priorly plasma treated (high surface energy) and a COP stamp with no plasma treatment (low surface energy).

The challenge with this treatment was revealed after punching since it would become problematic to entirely demold the PVA substrate. Since the substantial increase in surface energy of the COP stamp would allow for uniform coating, however, it resulted in either tear or stretch of the PVA substrate upon demolding, if the treatment was too long, (figure 11 a and b). Thus, it was concluded that the COP stamps needed the least time of plasma treatment possible (2 s), since this would still be enough to ensure efficient wetting of the stamp while minimizing demolging difficulty. Demolding difficulty was also reliant on other factors that will be further discussed in the next sections.

Throughout the usage of this coating method some coating defects prevailed. More specifically edge defects which consisted in variations in the thickness at the edges of the coated COP stamp. Particularly at the finishing coated edge of the stamp where the liquid would retract increasing the thickness in that region. This was due to the differences of surface tension between the stamp (low surface tension) and the plastic sheet underneath (high surface tension). This plastic sheet was used on top of the moving plate to prevent the excess liquid into the system vacuum, and so the stamp was placed on top. The coating distance required to go across both to ensure full coverage of the stamp along the possible coating width of 50 mm. Also, this minimized these edge defects, nevertheless these could never be entirely avoidable due to surface tension differences. After UV-assisted punching this defect would be cleared with this region staying wet meaning that hydrogel was not fully formed or punched, due to increased volume, (figure 11 c).

This defect showed higher significance at lower viscosities, as it was the case for the solution formulation with no Hb. This happened since the coating with this solution became mainly dominated by the surface tension, which meant that the capillarity forces overpowered any viscous forces from the fluid. To correct this effect different strategies could be applied, such as using sacrificial extra COP stamp. This by not using only the area of the pattern in the stamp to coat, as it was standard, but the entire 4-inch COP stamp that had 1 cm extra all around the pattern of COP. In addition, if the PVA substrate, after coating, was stacked in the opposite direction as the coating itself, it would push gradually away the extra liquid in the finishing edge towards the rest of the stamp, minimizing this nonuniformity defect.

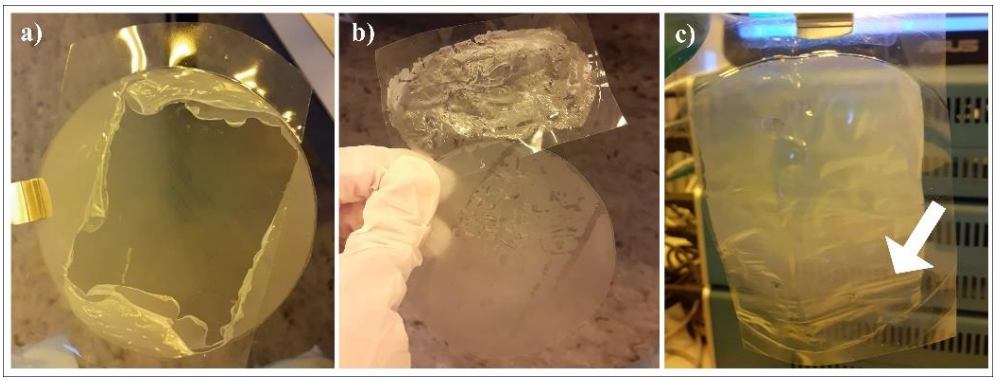

Figure 11 - Different results upon PVA demolding after UV-assisted punching. (a) is an unsuccessful demolding step (the stamp stayed connected to the PVA), (b) is more successful (full separation), but still not optimal, and (c) is successful although the resulting PVA substrate had some edge defects on the bottom (highlighted by the white arrow).

It is also relevant to point out that the COP stamps had the shaped microwells imprinted in its surface which might have played a role in the coating since it cannot be considered a flat COP foil. Studies have shown that the increase in micro-textures density, increases the adhesion to the coating to a substrate [38].This since there is an increase in the bonding area between the substrate and the coating. The same can be assumed in this study, playing a role in liquid distribution while coating. This can translate in an increase in thickness to do the heightened adhesion to the substrate.

3.3.1.1 PEG-based formulation without Hb

It was chosen a range of volumes to test, which initially had a superior gap height (0.36 mm) and superior volumes dispensed (100µL, 80µL, 70µL, 60µL, and 50µL), just as a starting point for testing. Then, by the end, lower volumes were dispensed (40µL, 35µL) with a lower gap height (0.24 mm). The coating speed was not further optimized due to the value used being a well-establish speed for uniform thin film coating. Additionally, the flow rate would change automatically according to the volume. The volume was progressively decreased to obtain the thinnest film possible while still ensuring uniform coating. From this optimization it was understood the existence of a range of limitations regarding the operating varied parameters, that will be fully discussed next.

Concerning the gap height parameter, since the COP stamp had a thickness ~0,20 mm, the gap had to be superior enough for the slot die coater head not to touch or consequently damage the stamp or slot die head. In addition, although the vacuum pressure could ensure that the COP stamp was as flat as possible on the plate, in this specific case it did not. Due to the plastic protecting sheet, that was just mentioned above. However, this meant that the gap height needed to compensate for any undesired bend that the stamps most probably had by increasing its value. With that said it the minimal gap height became of 0.24 mm, since less than that make the lip enter in contact with the stamp while coating. Thus, in reality the gap by subtracting the stamp thickness was ~0.04 mm from the stamp.

Furthermore, this parameter in combination with the volume dispensed needed to ensure the formation of a steady liquid curtain for the entire coating distance between the stamp and the slot die lip, as explained before in section 1.4.4. This meniscus stability was dependent of a crucial balance between the flow pressure and the shear forces present at the substrate-liquid interface [34]. The gap and the volume remained a constant influence in, not just, the liquid distribution, but also the resulting flow pressure at the lip. It was known that the gap height is inversely proportional to the flow pressure. In contrast the volume directly proportional to the flow pressure due to increase flow rate.

Since the goal was to arrive to the thinnest wet film possible, it was tested the lowest possible volume that could be dispensed, for the minimal gap height (0.24 mm) while still ensuring the formation of a steady downstream meniscus with the entire meniscus guide width (50 mm). This volume turned out to be 35µL as it corresponded to the limit in flow rate that allowed for uniform complete coverage of the stamp. Otherwise, if the volume for this gap height went lower or if for this volume the gap was higher, then these meniscus formation preconditions would not be met. Consequently, the downstream meniscus would be unstable during the coating, implicating that coating defects would occur. With one of the most common coating defects observed in this situation, being the neck in, that consisted in the gradual decrease in the coating width of the film across the coating distance [34].

3.3.1.2 PEG-based formulation with Hb

On Hb addition the viscosity of the solution increased proportionally with the increase of quantity added, as expected. This fluid viscosity also increased over time, since the Hb started losing functionality. With the increase in fluid viscosity the parameters had to be slightly adjusted to meet the preconditions for meniscus formation and stability. This since the interaction with the substrate would change for these formulations.

For the lowest Hb concentration in solution (1g/L) the parameters were kept the same (35µL of volume with a gap height of 0.24 µm) and it was visible that the formation of the meniscus became slightly easier than in the original formulation (no Hb). This was expected since, there was an increase of viscosity. However, this was not substantial, thus, the liquid distribution behaviour mostly resembled the original solution. It was still enough to offer a good balance of forces, forming a stable meniscus, uniform coating, (figure 12 c). More specially, a balance between the viscous forces in the fluid and the capillarity forces associated with the surface energy of the substrate. For the other two Hb concentrations (5g/L and 10g/L) an adjustment of parameters had to be done, since it was noticed that the viscous force became stronger than the capillary force of the downstream meniscus. This resulted in the occurrence of the rivulets, which consisted of a coating thickness variation and furthermore creating multiple smaller coating stripes. This defect can be seen in figure 12 b, and it is due to the nonuniform curvature of this meniscus, which transpired owning to a compromise of equilibrium between forces at the substrate-liquid interface resulting in 3D flow instability due to shear forces and flow pressure.[34] To elaborate, the viscosity affects liquid distribution inside the slot die coaters head along with the flow pressure. Flow pressure decreases with the increase of fluid viscosity. This directly reflects on the formation of the meniscus since it becomes increasingly harder to keep it stable during the coating for higher fluid viscosities.

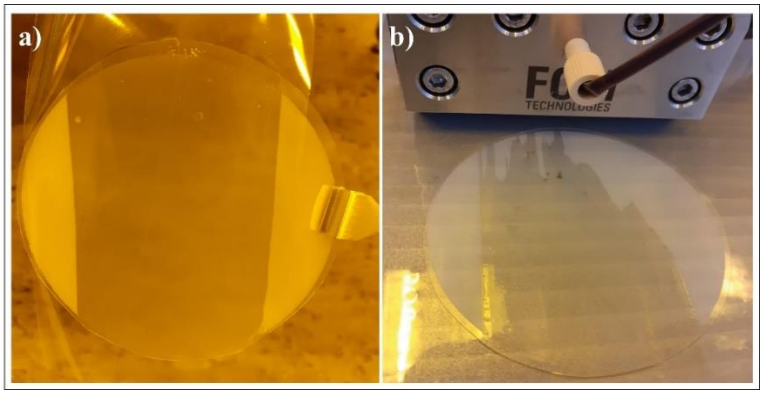

Figure 12 - Coating made with solutions without Hb or with the lowest Hb concentration (1g/L) resulting in a uniform coating (a) and coating defects occurring when coated with solutions with higher Hb concentration (5g/L and 10g/L) (b).

To correct this effect different parameters were varied but the gap was kept the same (0,24 mm). First it was added more volume, from 35µl to 40 µl, to compensate for the decreased flow pressure, which was able to ensure the full uniform coating. Nevertheless, theoretically, this could also be solved by the increase of the shear forces in order to compensate for the viscous force within the fluid. These forces were correlated to the movement of the plate which represents the speed of the coating process. Thus, it was also tested an increase of speed from 0,4 m/min to 0,6 m/min. However, this increase did not improve the display of these defects. One possible reason why was due to the fact that an increase in coating speed could result in a rise of air bubbles trapped within the coating film. This occurs as an air entrainment defect, which is usually expected from a discontinuity in the upstream meniscus (static point were the liquid meets the stamp, represented in the image in section 1.4.4, figure 3).

Lastly, defects also might have occurred due to occasional dry solution at the edges of the slot die coater meniscus guide. Particularly for the highest Hb concentration in solution, which contributed for a poor liquid distribution. The solution to this challenge was to clean this lip between coatings. In the future it could also been fixed by changing the formulation.

3.3.1.3 General assessment of the efficiency of the slot die coating process

Considering all the challenges just discussed above. As well as the fact that this coating step was essential for the next step of UV-assisted punching to obtain the final microgel shapes. It is important to conclude about the successfulness in achieving the desired thickness. With that said there is a theoretical study on the operating limits of slot die coating that can further prove the limitations faced during this optimization.

In advance it is also important to mention that the slot die coating tool assumes the liquids as non-Newtonians, discarding the effect of viscosity, so this study cannot be considered ideal. Nevertheless, it can still work as a theoretical reference.

According to Ding *et al*.,[33] there is a study that provides an equation to determines the minimum wet film thickness upon coating (Eq 1), where h_d is the downstream coating gap, and Ca is the capillary number, $\frac{\mu U}{\sigma_d}$. Furthermore, for Ca the σ_d is assumed as the surface tension in the atmosphere, as the downstream meniscus is always under atmospheric conditions (72mN/m [39]), the μ is the viscosity, and the U is the coating speed. Considering the original formulation, that it has a low fluid viscosity. Specifically, the same value of the fluid viscosity in water (~1mPa-s [40]) since this solution was prepared by 50%(w/v) in milli-Q water. Furthermore, knowing that the ideal t_{min} would be ~3 μm, and that the maximum coating speed allowed by this machine is 5 m/min it becomes possible to calculate the ideal theoretical height (h_d) in function of these values.

$$t_{min} = 0{,}67 h_d Ca^{2/3} \iff h_d = \frac{t_{min}}{0{,}67 Ca^{2/3}} \simeq 0{,}4\ mm \quad (Eq\ 1)$$

By comparing this theoretical gap height value to the one used after optimization (0,04 mm) it becomes clear that it would be impossible to use the same amount of volume (35µl) set as optimal. This since it would not meet the preconditions of the meniscus formation, probably resulting in a neck-in phenomenon. Thus, the volume would have to be increased and the minimal thickness compromised. Additionally, this is also assuming an extremely high coating speed. This would compromise the meniscus stability, as previously discussed above, due to air entrapment defects along with the substantial increase of shear forces applied to the liquid curtain.

Thus, this height would not be viable for this solution, under these conditions. This proves that the ultimate limitation in this optimization was the challenge in finding the correct balance between the competing forces, not accounted by the machine, and the operating parameters, set by the machine.

Lastly, there are some final aspects that must be addressed and that could have improved this optimization. First is the fact that the distribution of solution is very dependent on the geometry features of the different pieces in the slot die coater head. For instance, perhaps an increase of the meniscus guide width could have maximized the area of coating, as well as a change in the manifold design, which as a crucial impact on flow pressure. For example, in this specific work it was used a manifold that had a simple T-shaped design. This led to low solution flow rates closer to the lip, which consequently influenced the flow pressure and the formation of the meniscus. A change in this design could have further improved flow pressure.

3.3.1 Optimizing UV-NIL process

The results from the inspection of the microgel shapes on the PVA substrate, after UV-assisted punching, can undoubtedly reflect the challenges in coating thickness optimization. This due to the clear observation of a remaining hydrogel flash layer between and underneath the microgel shapes, (figure 13).

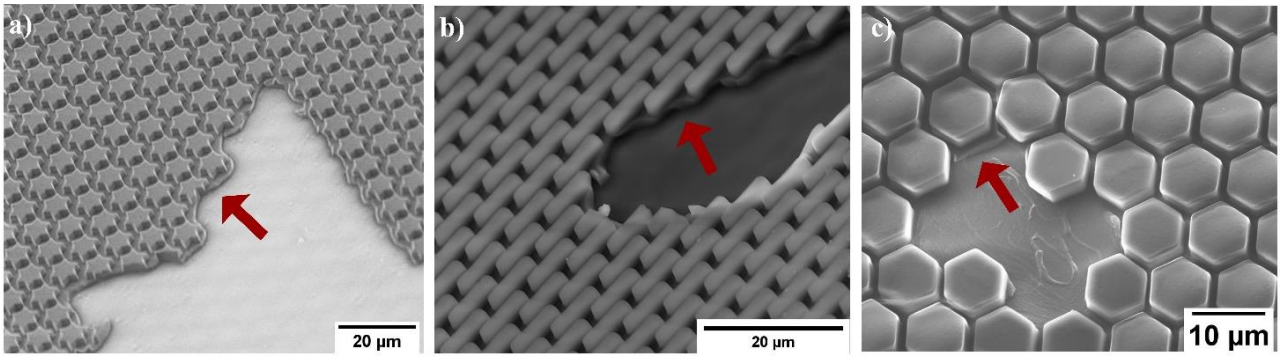

Figure 13 - Examples of SEM and SEM Tabletop topography inspections of the microgel shapes onto the PVA substrate that show a remaining thick hydrogel flash layer underneath the microgels.

Several different aspects contributed to the optimization of this process. The first were the challenges faced upon were related to PVA substrate demolding, as previously mentioned. Additionally, the aim of this method was to irradiate with UV light to initiate hydrogel formation at the same time as mechanical punching of the microgel shapes into the PVA substrate. This would allow for the microgel shapes to be transferred onto the PVA. Hence the importance of ensuring the proper operating parameters in the UV imprinter for the specific wet film thickness used. However, as discussed before, several limitations were continuously faced during the slot die coating process and therefore these will have to be taken into account in this part of the discussion.

Additionally, another concern during the PVA stacking step was that the rapid evaporation of the wet film, due to the small volume being dispensed. This resulted in sections of the stamp completely uncoated or specific microwells being poorly coated. Examples of this result can be found in appendix C.

To prevent this problem, the stacking of the PVA substrate onto the coated stamp had to be performed as fast and as evenly as possible, to not form any air bubbles. This turned out to be challenging at first but became more doable after some practice. Another two options would have been to use a small roll, by hand, or use the roll-to-plate (R2P), machine to stack the PVA uniformly. However, these solutions would also come with challenges regarding the difficulty of PVA demolding after punching, due to increased pressure. Owning to the increased adhesion between COP stamp and PVA substrate. Additionally, during the R2P method, the PVA foil separated from the COP stamp due to the low PVA thickness (~40 µm).

The first trials of slot die coating for high volumes (from 100 to 50 µl), were under 4 bars and a UV time of 20 mins during the UV-assisted punching process. However, after PVA dissolution it was seen in the microscope that the microgels were mainly connected, nonideal coating thickness, which was why the coating volume was decreased to 35µl. By using the same operating parameters, however, for this decreased volume it became incredible challenging to demold. This was expected as the thinnest wet film would result in greater adhesion between the COP stamp and the PVA substrate.

Nevertheless, it needs to be reinforced that it became almost impossible to fully demold the PVA substrate. The parts that demolded, edges, under inspection afterwards showed stamp failure. This since the microwells came attached to the microgel shapes on the PVA substrate, figure 14, due to stamp damage. This problem only appeared with the rods and hexagon microgels transferred onto PVA. This since these were the the patterns with denser arrays and thus, harder to demold.

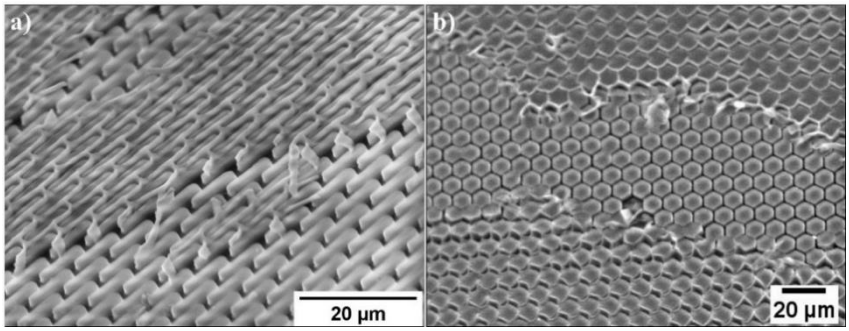

Figure 14 - Examples of COP structures attached to the microgel shapes after PVA demolding upon SEM Tabletop inspection.

In optimization process itself consisted in decreasing gradually both the UV time and the pressure applied. It was concluded that the UV time could be significantly decreased to 2 or 1 mins without compromising the full crosslinking of the coated formulations into hydrogels. This due to the fact that small volumes were used to coat, and that the transparent substrate, PVA, played its role perfectly and led the light pass through easily. It also proves that the concentrations used to prepare the formulations were accurate, as the photoinitiation process was successful. The pressure was also decreased to half, however, played a more crucial role in the mechanical punching step. It also directly influenced these demolding challenge as a decrease in pressure would improve the demolding step. It is important to remember that for the two formulations with higher Hb concentrations (5g/L and 10g/L) the final optimal parameters had to be adjusted. This since the volume used in coating was increased, a so these parameters were slightly increased. In addition, has it will be further discussed in the next section, the differences between the arrays also played a role in the optimization of parameters. In the end, the parameters were optimized to overcome the demolding challenge, as well as to ensure mechanical punching and hydrogel formation for each microgel shape and for each formulation.

The details of these optimizations can be seen in x of the appendix C.

3.3.1.1 Final microgel shapes

From the PVA substrate inspection, seen in figure 15 and 16, after the final process it can be observed that the microgels shapes have the desired shape show good geometric features for all four formulations. This means that the introduction of Hb into the polymerization synthesis did not compromise the formation of microgel shapes for the concentrations used.

Additionally, although for the most part there was a great yield of microgel shapes onto the PVA substrate this was never 100%, since there were always small regions across the PVA substrate with no microgels shapes or with damaged ones. This would be proportional to the difficulty in demolding, that could result in microgels staying in the COP stamp, or direct damage to the PVA itself. It would also be related to

poor handling of the resulting PVA substrate after demolding. If the demolding step was successful then this would not be significant considering the great quantity of microgels punched, however it needs to be mentioned.

The rods microgel shapes, showed an increase in breakage within the microstructure itself. This was due to their elongated shape (reduced width) in comparison to the other less elongated microgel shapes, that keep their shapes intact after PVA demolding.

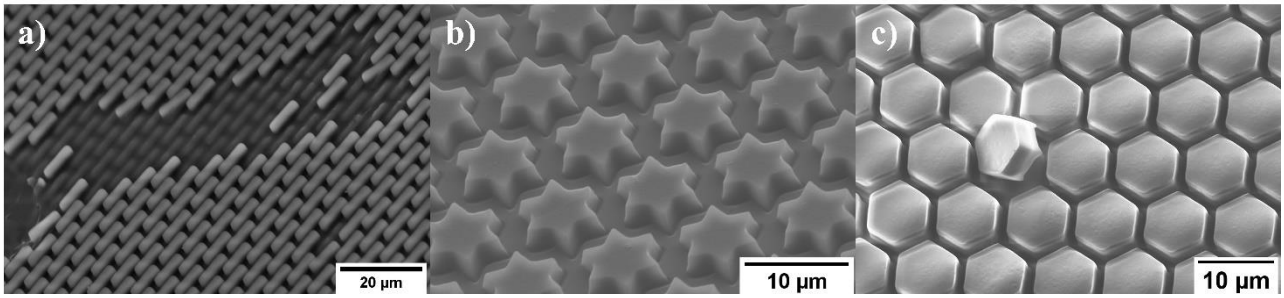

Figure 15 - SEM and SEM Tabletop topography inspections of the different microgel shapes, rods (a), stars (b), and hexagons (c) onto the PVA substrates made from the original formulations (without Hb).

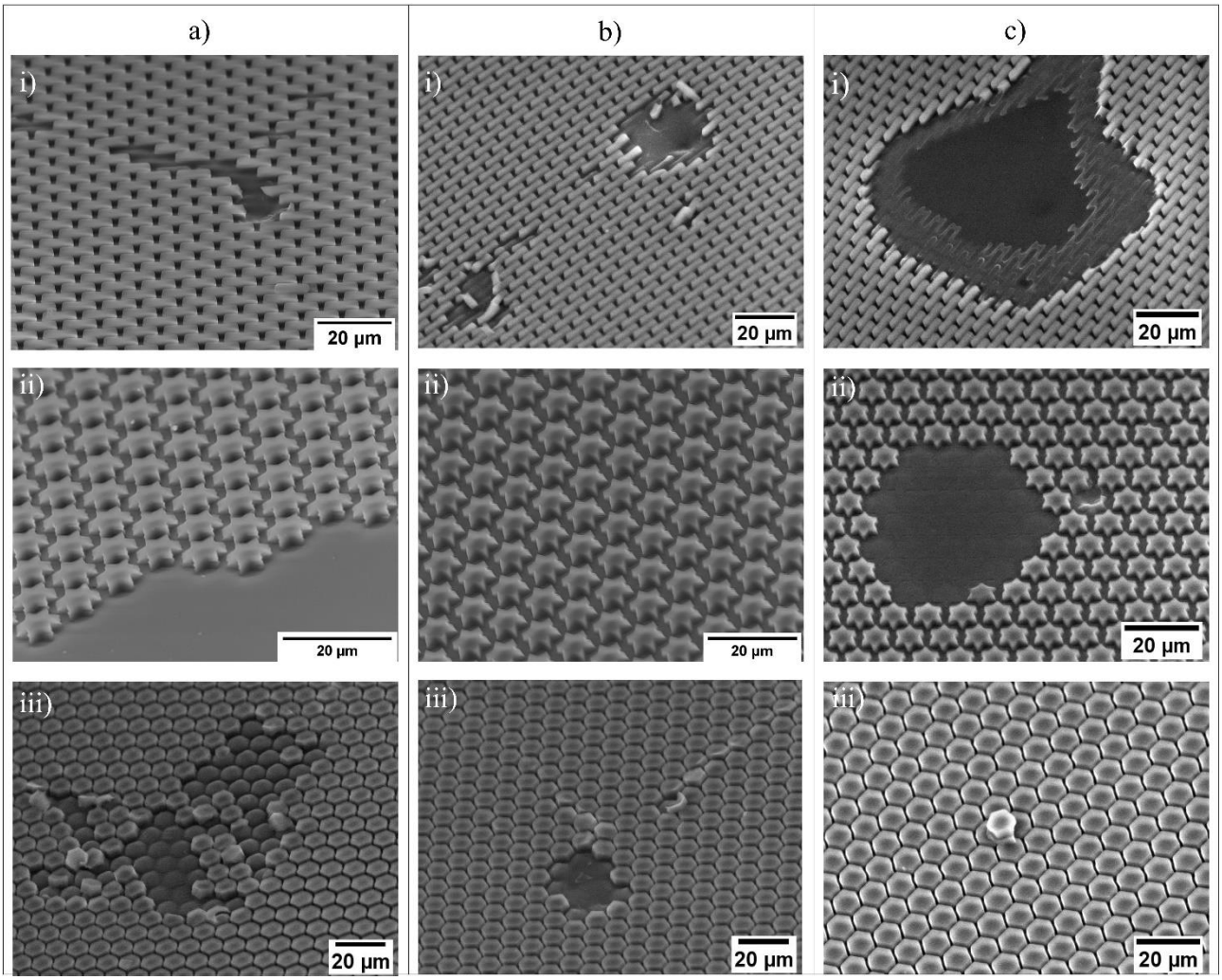

Figure 16 - SEM and SEM Tabletop topography inspections of the different microgel shapes, rods (i), stars (ii), and hexagons (iii) onto the PVA substrates made from the formulations with various concentrations of Hb. (a) 1g/L, (b) 5g/L, and (c) 10g/L.

From the PVA substrate the height of the final hydrogel microparticles, was also measured for the rods, star and hexagon microgels shapes, table 5. It was also taken the respective 3D topographies and height profile plots, along with the respective images of the final microgel shapes after harvest (PVA dissolution) figure 17. Additionally, the lack of an 3D topography of this shape stands from difficulties in adjusting the light in the optical profilometer for these specific features due to bends of the PVA substrate itself. Nevertheless, the height of these microgels was still measured.

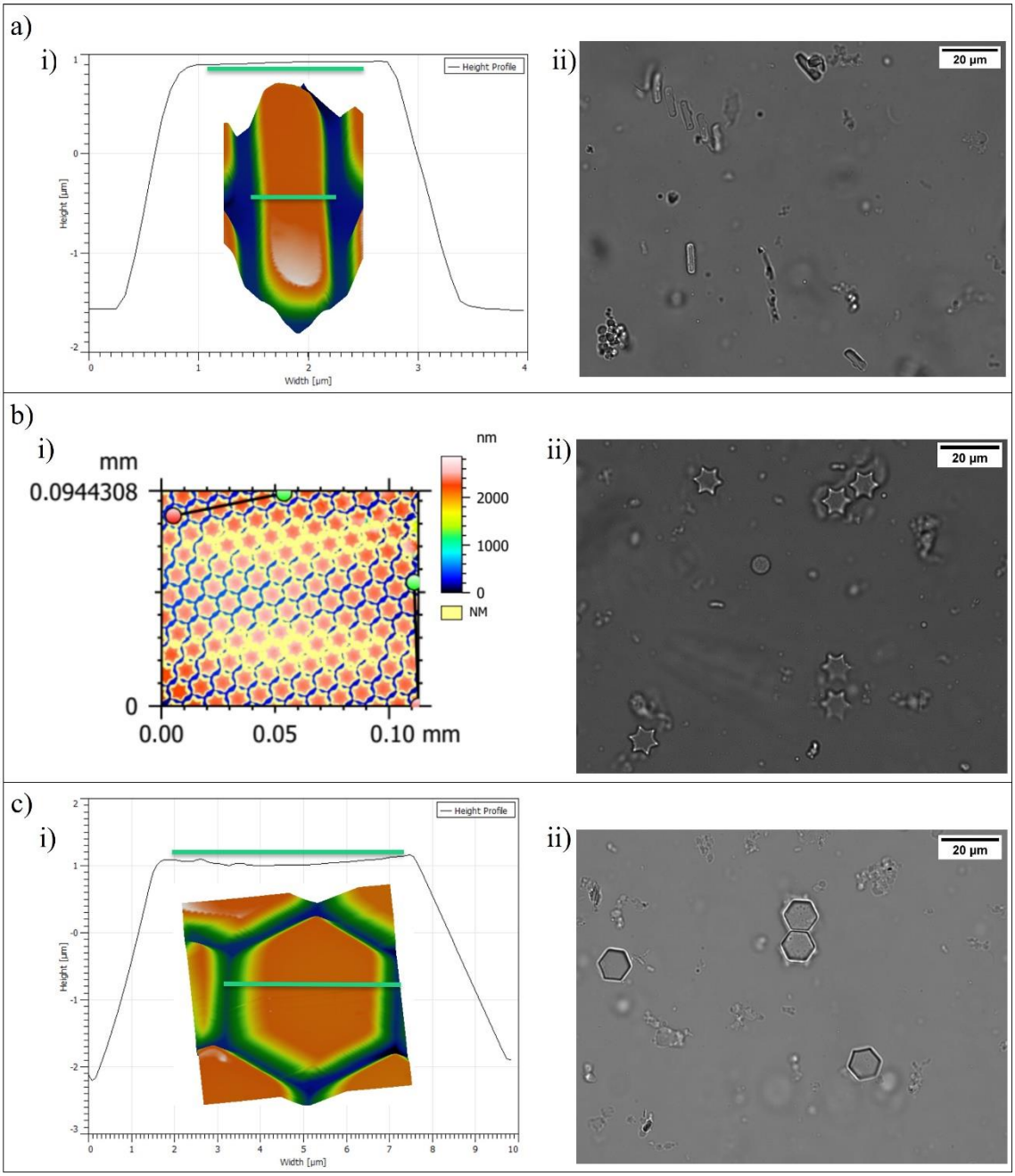

Figure 17 - Microgel shapes onto PVA substrate topography inspection (i), through 3D images and correspondent height profile plots, and microscopic inspection of microgel shapes after PVA dissolution (ii). For the different shape rods (a), stars (b), and hexagons (c).

It is important to understand the difference between embossing and punching in this analysis. Embossing focuses only obtaining the desired pattern in the stamp on the substrate, resulting in the microgel shapes as the pattern imprinted. The mechanical punching focused on the pattern in the stamp cutting through the any flash layer into the PVA substrate. In this work it was observed clear embossing obtaining good microgel shape features. However, trying to confirm the mechanical punching step was more complex, as this was not as clear

to observe. The flash layer thickness played a major role since it could act as a barrier to punching if is too thick.

From these results it can be observed was the microgels shapes for the most part was still connected, after harvest, resulting in a very small yield of individual microgel shapes. More images of the resulting connected microgel shapes can be found in appendix C. Hence, proving that the mechanical punching was not successful enough to ensure the separation of these microgels or the PVA was not fully dissolved. The first reason was directly dependent from the thickness of the flash layer, as above explain. This was a consequent of the nonoptimal thickness of the wet film priorly coated. Additionally, it was also a consequence of the reduction of pressure during UV-assisted punching that allowed an easier demold. Thus, it was concluded that there was a possible trade-off between achieving mechanical punching or successfully demolding the PVA substrate. In addition, the existence of mechanical punching could also be seen observing the heigh profile plots. This as if there were then these plots would have a dent in height, punching depth closer to the bottom of the sidewalls of these microgels, proving punching.

Table 5 – Summarized final height or depth measurements of each structure.

Shapes	**Rods**	**Hexagons**	**Stars**
Height of Si microstructures (µm)	2,66 ± 0,18	3,70 ± 0,03	2,48 ± 0,07
Depth of COP microwells (µm)	2,44 ± 0,24	3,46 ± 0,31	2,38 ± 0,19
Height of PEG microgels (µm)	**2,43 ± 0,07**	**3,72 ± 0,09**	**2,26 ± 0,06**

By comparing the final height measurements of the three microgel shapes with the prior height and depth results from the structures in Si masters and COP stamps, respectively, it can be concluded that there was a good final replication fidelity of the initially fabricated Si microstructures.

Additionally, in general hydrogels can swell depending on their network design. In this work it was not observed any swelling of these microgel shapes in water, thus they maintain their shape. This means that the final aspect ratio of these microgel shapes would still be 3:1 as aimed for.

Finally, to conclude about the full quality of this fabrication method that led to the microgel shapes the possible fabrication yield was calculated. Firstly, an estimated quantity of microwells on the stamp based on the quantity of rods in the initial periodical circular design was calculated, determined as ~130 000 microwells. To simplify this value was assumed to be the same for all the designs (rods, stars and hexagons patterns) and therefore it represented the value of 100% of yield. Nevertheless, as it was discussed before, the coating is limited by the lip width of 50 mm and knowing that the diameter of the COP stamp is 80 mm an approximated area can be calculated. From there it could be determined that the number of wells coated is ~ 103 450, which can be assumed as the same number of UV imprinted microparticles. The final calculated fabrication yield result was the following:

$$Fabrication\ yield = \frac{the\ number\ of\ UV\ imprinted\ microparticles}{the\ number\ of\ microwells\ on\ the\ stamp} \times 100 \simeq 80\%$$

Nevertheless, this did not account for the demolding and handling microparticle losses, that were mentioned before. Furthermore, this yield was not the achieved, but rather the ideal, if this process had been fully properly optimized to overcome all the challenges discussed before. Therefore, the conclusion to take from this is that these last fabrication processes, slot die coating combined with UV-assisted punching, required more time to explore different routes of further optimization in order to reach better results.

4

Conclusions and Future Perspectives

This project was mainly focus on the understanding of the different fabrication methods used to produce three different shapes of microgel shapes (rods, stars and hexagons), to work as possible surrogates for Hb encapsulation (artificial RBCs). It is believed that this aim was achieved, even though the ultimate goal of obtaining a good yield of separated microgel shapes was not fully reached. Furthermore, this study proved the potential of these fabrication methods in achieving the desired features of the diverse microgels. More specifically features within the same size range as RBCs (aspect ratio 4:1).

The fabrication of the Si masters with the different patterns previously designed in CleWin was overall very successful. This since it was possible to obtain a high resolution of the patterns prepared throughout the UV lithography parameters used, that led to quality photoresist masks. This consequently offered a great starting point for the etch of the oxide layer. Although this etching process did not offer incredible results in terms of the smoothest sidewalls surface, it offered good selectivity. In general, it was efficient enough for the purpose of this etch, which was to create a mask for the final and crucial Si etch step.

From the optimization of the Si etch process (CORE sequence) it was obtained excellent 3D features of the final microstructures across the Si wafers. This was detrimental since these were the original templates that led to the final microgel shapes. Additionally, it resulted in an average etch depth ~3µm for all the patterns along with lengths of ~10 µm. This ensured the desired aspect ratio of 3:1 for every shaped Si microstructure.

The results from the production of the COP stamps by hot embossing, were also promising. There were not any major distortions or deformations upon the demolding of the Si master templates that compromised the final replication of the inverted patterns onto the COP foil. Additionally, the operating parameters chosen to emboss this material demonstrated to be in the proper range. This enabled a high replication fidelity and uniformity throughout the entire stamp. Lastly, this method showed high reproducibility since the masters had great durability and the process itself was simple and fast.

The main challenges faced during this project were related to the final fabrication steps, slot die coating combined with UV-assisted punching. By doing an overview on the factors that most affected the results it can be highlighted the following three: thickness and uniformity of the coating, UV exposure time, and pressure applied during embossing. Furthermore, for the thickness of the wet film, it was detrimental the surface energy of the COP stamp, the different viscosities between formulations used. As well as the main operating parameters of the machine (speed, gap and volume), and the specific geometry of the slot die coating head itself. It was concluded that the uniformity and efficiency of the coating was a direct result of the stability in the meniscus (upstream and downstream) formation between the lip and the substrate. This subsequently relied on the proper balance between the parameters and the competing forces (mainly shear, viscous, and capillary forces). With that said, it is believed that the uniformity in the coating was successfully achieved for all formulations although the thickness reached optimization limitations due to lack of time. In addition, it was also proven that there was a direct trade-off between mechanical punching and PVA demolding. Along with the success of mechanical punching being limited by the nonoptimal thickness in coating, which compromised the final yield of individual microgel particles.

Regarding the results from the diverse formulations with a range of fluid viscosities (different concentrations of Hb) it was concluded this affected the coating uniformity and thickness. However, it still allowed for the complete crosslinking into hydrogels during UV-assisted punching, as well as shape retention. From the coating results it can be also concluded that for Hb concentrations greater that 10g/l in formulation, it would be gradually harder to achieve a uniform thin film coating. This due to the increasing occurrence of defects. Furthermore, a greater increase of concentration would likewise, eventually, compromise the formation of the hydrogel. This due to the how much the network of the hydrogel could encapsulate without losing physical integrity. Thus, it can be concluded that from the results achieved it can be anticipated that this encapsulation thought these methods would arrive to a pivotal limitation.

If this work was to continue there were a few proposals for further optimization to try to overcome the challenges faced during these specific last processes. Firstly, it should be attempted to change the geometry of the slot die coaters head, more specifically the manifold, to a different shape that could promote an increase of flow pressure. This would adjust the liquid distribution inside the head, to compensate for the fluid viscosity with Hb encapsulated. Additionally, a wider meniscus guide (lip) should be used so the coating could be done for the entire stamp with just one coating layer, increasing the efficiency.

Regarding the UV-assisted punching process it could be tried to alter the order of the stack, by putting the stamp on top instead of the PVA substrate, since this material is also transparent. Hence, under the correct operating parameters this adjustment could perhaps allow for better mechanical punching while still ensuring hydrogel formation and easy demolding of the PVA afterwards.

Furthermore, if the optimization steps just mentioned were fully successful and hence the coating thickness and the punching obtained ideal. Then it would be possible to obtain individual microgel shapes with the desired features after harvest. Assuming this firstly it would be done a complete proper yield determination and analysis of how reproducible this fabrication was, by attempting repetition of production. Afterwards the following future work would be developed to study how successful was the Hb encapsulation and if these microgel shapes were compatible with endogenous RBCs. The former would be proven through a haemolysis test in vitro, that consisted in an assessment of the behaviour of RBCs around the microgels with and without Hb encapsulated. Regarding the efficiency of the Hb encapsulation itself the functionality could be proven by characterizing the resulting microgel shapes with Hb encapsulated in suspension using dynamic light scattering (DLS). Moreover, this light scattering assay, would be aiming to find an absorption peak around 412 nm, which is the peak that corresponds to the oxygenated Hb in endogenous RBCs. Additionally, these two results would be compared between the three different shapes produced in order to conclude if the shape played any role in the efficiency of these artificial RBCs.

Another future aim would be to test the possible size limits of these microgel shapes, by going back to the original design and decreasing the features of each shape. Then proceeding with the same fabrication steps to analyse the possible size limitations of these methods. This target comes from the fact that nanoparticles have shown longer circulation times than microparticles.

The reduction of feature sizes in this specific field of study could be incredible relevant to improve biocompatibility of these microgel shapes, not just, with to be used as artificial RBCs, but also, for other drug delivery applications. In summary, the future for the fabrication of hydrogel microparticles and nanoparticles is very bright and therefore it is believed that it will continue to be an extensive area of research for biomedical applications.

BIBLIOGRAFIA

[1] C. Coll-Satue, S. Bishnoi, J. Chen, and L. Hosta-Rigau, "Stepping stones to the future of haemoglobin-based blood products: Clinical, preclinical and innovative examples," *Biomater. Sci.*, vol. 9, no. 4, pp. 1135–1152, 2021, doi: 10.1039/d0bm01767a.

[2] C. Bialas, C. Moser, and C. A. Sims, "Artificial oxygen carriers and red blood cell substitutes: A historic overview and recent developments toward military and clinical relevance," *J. Trauma Acute Care Surg.*, vol. 87, no. 1S Suppl 1, pp. S48–S58, 2019, doi: 10.1097/TA.0000000000002250.

[3] A. Sen Gupta, "Role of particle size, shape, and stiffness in design of intravascular drug delivery systems: Insights from computations, experiments, and nature," *Wiley Interdiscip. Rev. Nanomedicine Nanobiotechnology*, vol. 8, no. 2, pp. 255–270, 2016, doi: 10.1002/wnan.1362.

[4] S. Grijalvo, J. Mayr, R. Eritja, and D. D. Díaz, "Biodegradable liposome-encapsulated hydrogels for biomedical applications: A marriage of convenience," *Biomater. Sci.*, vol. 4, no. 4, pp. 555–574, 2016, doi: 10.1039/c5bm00481k.

[5] N. Kapate, J. R. Clegg, and S. Mitragotri, "Non-spherical micro- and nanoparticles for drug delivery: Progress over 15 years," *Adv. Drug Deliv. Rev.*, vol. 177, 2021, doi: 10.1016/j.addr.2021.05.017.

[6] J. G. Mohanty, E. Nagababu, and J. M. Rifkind, "Red blood cell oxidative stress impairs oxygen delivery and induces red blood cell aging," *Front. Physiol.*, vol. 5 FEB, no. February, pp. 1–6, 2014, doi: 10.3389/fphys.2014.00084.

[7] X. Li *et al.*, "Cetuximab modified collagen scaffold directs neurogenesis of injury-activated endogenous neural stem cells for acute spinal cord injury repair," *Biomaterials*, vol. 137, pp. 73–86, 2017, doi: 10.1016/j.biomaterials.2017.05.027.

[8] P. W. Buehler, F. D'Agnillo, and D. J. Schaer, "Hemoglobin-based oxygen carriers: From mechanisms of toxicity and clearance to rational drug design," *Trends Mol. Med.*, vol. 16, no. 10, pp. 447–457, 2010, doi: 10.1016/j.molmed.2010.07.006.

[9] W. H. Reinhart, N. Z. Piety, J. S. Goede, and S. S. Shevkoplyas, "Effect of osmolality on erythrocyte rheology and perfusion of an artificial microvascular network," *Microvasc. Res.*, vol. 98, pp. 102–107, 2015, doi: 10.1016/j.mvr.2015.01.010.

[10] H. Sakai, K. Sou, H. Horinouchi, K. Kobayashi, and E. Tsuchida, "Review of hemoglobin-vesicles as artificial oxygen carriers," *Artif. Organs*, vol. 33, no. 2, pp. 139–145, 2009, doi: 10.1111/j.1525-1594.2008.00698.x.

[11] X. Duan and Y. Li, "Physicochemical characteristics of nanoparticles affect circulation, biodistribution, cellular internalization, and trafficking," *Small*, vol. 9, no. 9–10, pp. 1521–1532, 2013, doi: 10.1002/smll.201201390.

[12] S. Muro *et al.*, "Control of endothelial targeting and intracellular delivery of therapeutic enzymes by modulating the size and shape of ICAM-1-targeted carriers," *Mol. Ther.*, vol. 16, no. 8, pp. 1450–1458, 2008, doi: 10.1038/mt.2008.127.

[13] Z. Zhou *et al.*, "Linear-dendritic drug conjugates forming long-circulating nanorods for cancer-drug delivery," *Biomaterials*, vol. 34, no. 22, pp. 5722–5735, 2013, doi: 10.1016/j.biomaterials.2013.04.012.

[14] G. Wang *et al.*, "High-relaxivity superparamagnetic iron oxide nanoworms with decreased immune recognition and long-circulating properties," *ACS Nano*, vol. 8, no. 12, pp. 12437–12449, 2014, doi: 10.1021/nn505126b.

[15] N. A. Peppas, J. Z. Hilt, A. Khademhosseini, and R. Langer, "Hydrogels in biology and medicine: From

molecular principles to bionanotechnology," *Adv. Mater.*, vol. 18, no. 11, pp. 1345–1360, 2006, doi: 10.1002/adma.200501612.
[16] T. K. Merceron and S. V. Murphy, *Hydrogels for 3D bioprinting applications*. Elsevier Inc., 2015.
[17] J. Ulbricht, R. Jordan, and R. Luxenhofer, "On the biodegradability of polyethylene glycol, polypeptoids and poly(2-oxazoline)s," *Biomaterials*, vol. 35, no. 17, pp. 4848–4861, 2014, doi: 10.1016/j.biomaterials.2014.02.029.
[18] P. Sensharma, G. Madhumathi, R. D. Jayant, and A. K. Jaiswal, "Biomaterials and cells for neural tissue engineering: Current choices," *Mater. Sci. Eng. C*, vol. 77, pp. 1302–1315, 2017, doi: 10.1016/j.msec.2017.03.264.
[19] H. Zhang, J. K. Jackson, and M. Chiao, "Microfabricated Drug Delivery Devices: Design, Fabrication, and Applications," *Adv. Funct. Mater.*, vol. 27, no. 45, pp. 1–31, 2017, doi: 10.1002/adfm.201703606.
[20] S. Aryal, H. Park, J. F. Leary, and J. Key, "Top-down fabrication-based nano/microparticles for molecular imaging and drug delivery," *Int. J. Nanomedicine*, 2019.
[21] P. Naulleau, "Optical lithography," in *Comprehensive Nanoscience and Nanotechnology*, 2019.
[22] J. del Barrio and C. Sánchez-Somolinos, "Light to Shape the Future: From Photolithography to 4D Printing," *Adv. Opt. Mater.*, vol. 7, no. 16, 2019, doi: 10.1002/adom.201900598.
[23] Y. Liu, P. F. Eng, O. J. Guy, K. Roberts, H. Ashraf, and N. Knight, "Advanced deep reactive-ion etching technology for hollow microneedles for transdermal blood sampling and drug delivery," *IET Nanobiotechnology*, vol. 7, no. 2, pp. 59–62, 2013, doi: 10.1049/iet-nbt.2012.0018.
[24] H. Microfabrication and M. Huff, "Recent Advances in Reactive Ion Etching and Applications of," 2021.
[25] F. Santos and D. Q. B. F. C. Ul, *Mass spectrometry Mass spectrometry*, vol. 1040, no. 2. INC, 2016.
[26] V. Thi Hoang Nguyen *et al.*, " The CORE Sequence: A Nanoscale Fluorocarbon-Free Silicon Plasma Etch Process Based on SF 6 /O 2 Cycles with Excellent 3D Profile Control at Room Temperature ," *ECS J. Solid State Sci. Technol.*, vol. 9, no. 2, p. 024002, 2020, doi: 10.1149/2162-8777/ab61ed.
[27] K. Mohamed, *Nanoimprint lithography for nanomanufacturing*, vol. 1–5. Elsevier Ltd., 2019.
[28] S. S. Deshmukh and A. Goswami, "Hot Embossing of polymers - A review," *Mater. Today Proc.*, vol. 26, no. xxxx, pp. 405–414, 2019, doi: 10.1016/j.matpr.2019.12.067.
[29] V. R. Sastri, *Commodity Thermoplastics*. 2014.
[30] B. Y. Joo, S. H. Rhim, and S. I. Oh, "Micro-hole fabrication by mechanical punching process," *J. Mater. Process. Technol.*, vol. 170, no. 3, pp. 593–601, 2005, doi: 10.1016/j.jmatprotec.2005.06.038.
[31] N. M. Fabrication, "Micromechanical Punching : A Versatile Method for," pp. 1–9, 2021.
[32] S. Mallakpour and S. Rashidimoghadam, *Poly(vinyl alcohol)/carbon nanotube nanocomposites*. Elsevier Ltd, 2017.
[33] X. Ding, J. Liu, and T. A.L.Harris, "A Review of the Operating Limits in Slot die Coating Processes," *Wiley Online Libr.*, 2016, doi: 10.1002/aic.
[34] Ossila, "Slot die Coating Theory." [Online]. Available: https://www.ossila.com/pages/slot-die-coating-theory. [Accessed: 04-Sep-2022].
[35] R. Patidar, D. Burkitt, K. Hooper, D. Richards, and T. Watson, "Slot-die coating of perovskite solar cells: An overview," *Mater. Today Commun.*, vol. 22, p. 100808, 2020, doi: 10.1016/j.mtcomm.2019.100808.
[36] A. Cherala, P. N. Pandya, K. M. Liechti, and S. V. Sreenivasan, "Extending the resolution limits of nanoshape imprint lithography using molecular dynamics of polymer crosslinking," *Microsystems Nanoeng.*, vol. 7, no. 1, 2021, doi: 10.1038/s41378-020-00225-y.
[37] I. Kourmpetis *et al.*, "Gradient-temperature hot-embossing for dense micropillar array fabrication on thick cyclo-olefin polymeric plates: An example of a microfluidic chromatography column fabrication," *Micro Nano Eng.*, vol. 5, no. July, p. 100042, 2019, doi: 10.1016/j.mne.2019.100042.
[38] Z. Zhang, W. Lu, W. Feng, X. Du, and D. Zuo, "Effect of substrate surface texture on adhesion performance of diamond coating," *Int. J. Refract. Met. Hard Mater.*, vol. 95, p. 105402, 2021, doi: 10.1016/j.ijrmhm.2020.105402.
[39] Nanoscience Instruments, "Surface and Interfacial tension." [Online]. Available: https://www.nanoscience.com/techniques/tensiometry/surface-interfacial-tension/.
[40] Y. Zhao, D. Zhao, Y. Zhong, and Y. Zhao, "The Viscosity of Oil Influence on the Working Characteristics of Electric Submersible Pump under Variable Speed," *IOP Conf. Ser. Earth Environ. Sci.*, vol. 661, no. 1, 2021, doi: 10.1088/1755-1315/661/1/012023.

A

An Appendix – Introduction

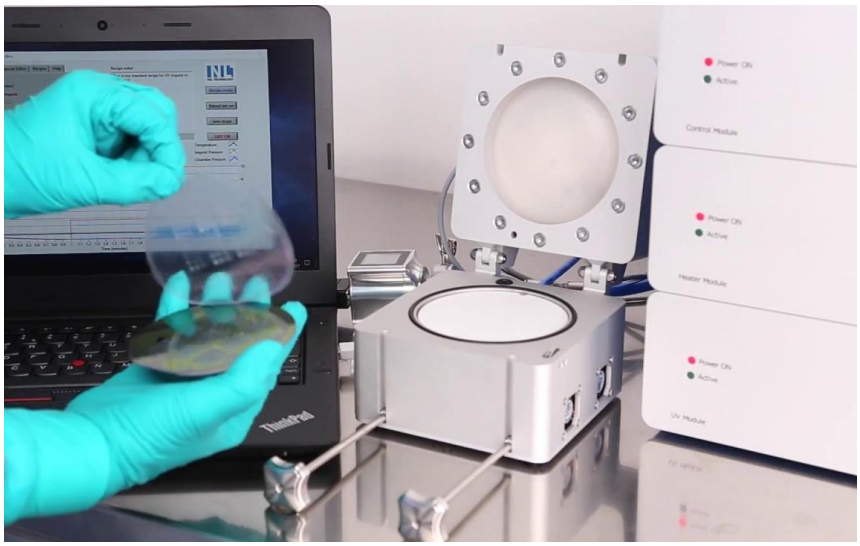

Figure 1 - NIL process tool.

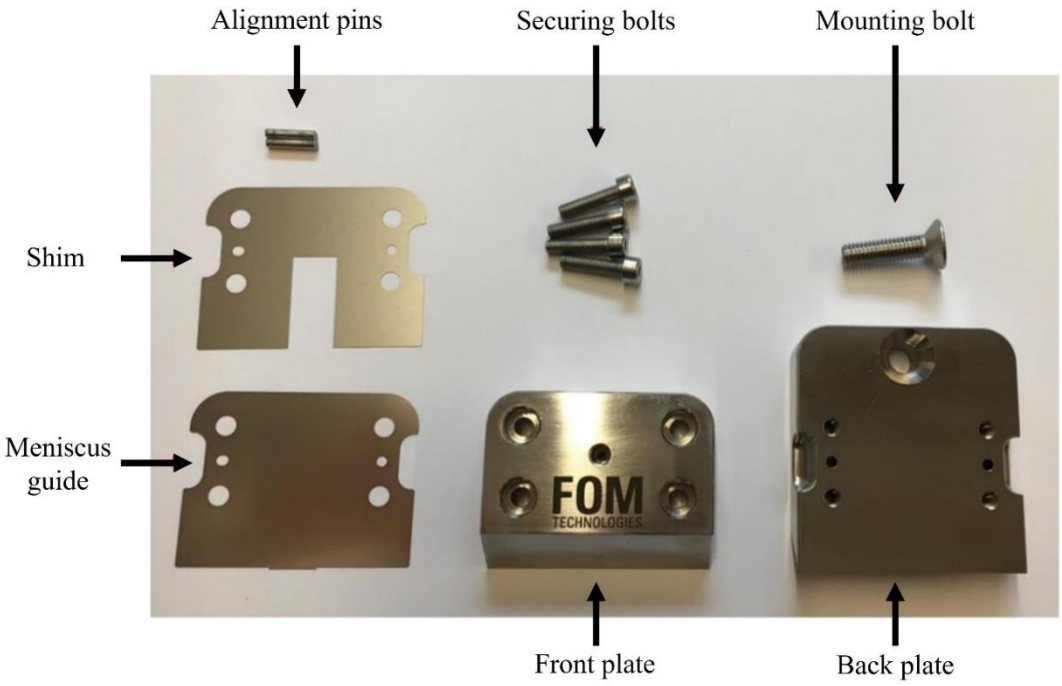

Figure 2 - Slot die head's different pieces.

B

ANOTHER APPENDIX - METHODS AND MATERIALS

B.1 PEB-based formulations

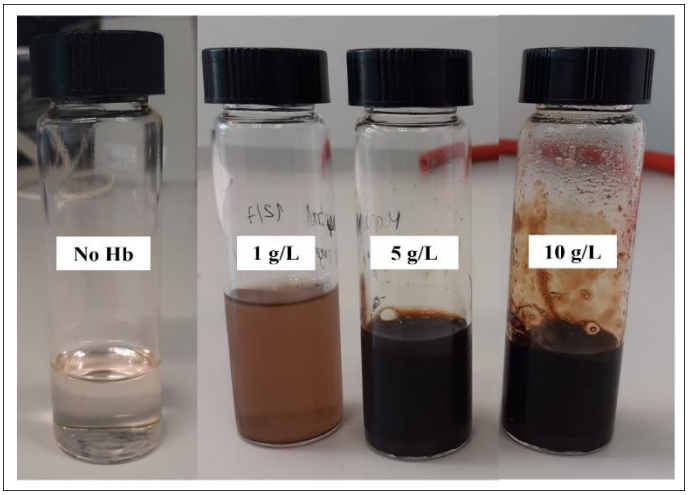

Figure 3 - All four different prepared formulations after a few days.

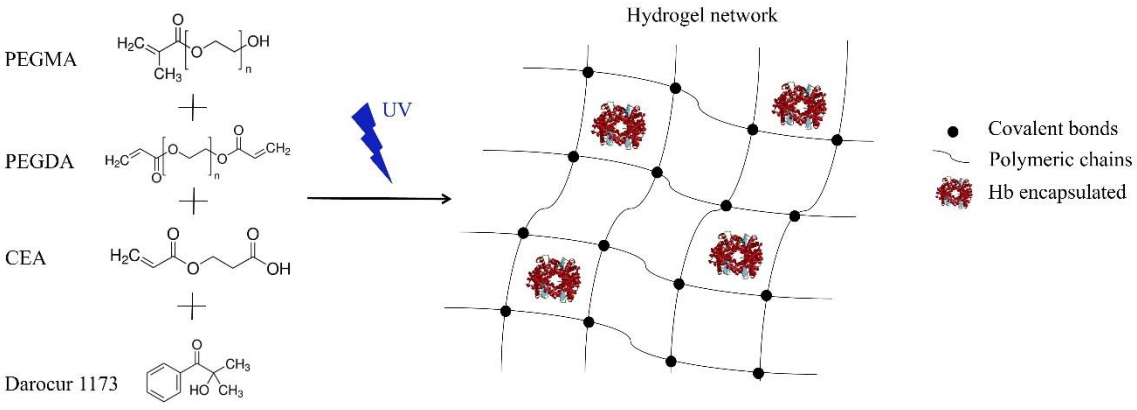

Figure 4 - Illustration of hydrogel network formation with Hb encapsulated.

B.2 Si masters

Si etch process constant operating parameters:

microCORE	Step	Time	Valve	O2	SF6	Platen
CPR		sec	%	sccm	Sccm	W
Oxidize	O	10	3	200	0	40
Remove bottom	R	10	100	0	5	40
Etch delay	E1	2	4	0	350	40
Etch	E2	Ra	4	0	350	300

Si etch process parameters varied during optimization (Centre point runs, COP):

CPRs	1	2	3	4	5 (Final)
N° of cycles	25	61	52	54	54
Ramping (Ra)	0-15s	0-15s	0-8s	0-2s	15s
Final time	10m10s	29m52s	22m28s	22m29s	22m30s

Si etch process parameters varied during optimization (Centre point runs, COP):

O_2 Plasma		**Flow**	200 sccm
		Power	250 w
		Time	300s
Repeated 4 times	**Chemical 1**	**Name**	FDTS2
		Line no.	2
		Cycles	4
		Pressure	0,5 Torr
	Chemical 2	**Name**	Water
		Line no.	1
		Cycles	1
		Pressure	18 Torr
	Processing	**Time**	900s
	Purge	**Cycles**	5

B.3 UV-assisted punching process parameters

To compensate for this demolding challenges of the PVA substrate, the parameters were optimized by gradually from the initial ones, by decreasing time of UV exposure and the pressure applied. Until it was reached the results that ensured the easiest demolding while still trying to exhibiting mechanical punching and hydrogel formation for each array. Additionally, the initial step of this method where no irradiation was occurring, but pressure was being applied was decreased to 0 mins, thus decreasing the adhesion between the COP stamp and the PVA substrate even further.

Initial process parameters:

Vacuum	125 bars
Time with UV	20mins (power 100%)
Time without UV	1min
Pressure	4 bar

Optimization process parameters using the rods COP stamp:

Pressure (bars)	**Time with UV (mins)**
3	15
2	15
2	10
2	5
2	2
1,5	1

Furthermore, between the three COP stamps used (rods, stars and hexagons), there had to be some adjustment due to differences in difficulty upon demolding, These optimizations were made with the original formulation (no Hb) and also could applied for the formulation with the lowest Hb concentration (1g/L). However, for the formulations with higher Hb concentration (5g/L and 10g/L), another adjustment had to be made.

Final process parameters for each COP stamp using the original formulation (no Hb) and the formulation with 1 g/ L of Hb:

	Pressure (bars)	**Time with UV (mins)**
Rods	1,5	1
Hexagons	1,5	1
Stars	2	4

Final process parameters optimized for each COP stamp using the other two Hb formulations (5g/L and 10 g/L):

	Pressure (bars)	Time with UV (mins)
Rods	2	2
Hexagons	2	2
Stars	3	4

B.4 Harvest of microgel shapes from PVA substrate

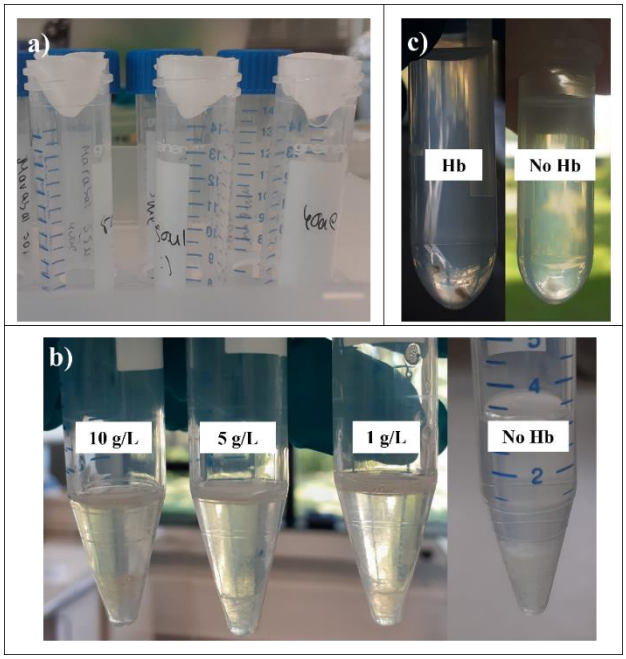

Figure 5 - Last steps to harvest the microgel shapes. With the following order: b) PVA dissolution, a) filtration, and c) small pellet of microgel shapes obtained after centrifugation.

C

ANOTHER APPENDIX - RESULTS AND DISCUSSION

Measuments of the features in each pattern (rods, hexagons, and stars arrays) after development:

Patterns	Rods	Hexagons	Stars	
Length (µm)	9,95 ± 0,05	9,83 ± 0,08	9,43 ± 0,07	
Width (µm)	2,31 ± 0,06	8,71 ± 0,05	8,10 ± 0,07	
Distance (µm)	1,17 ± 0,08	1,05 ± 0,05	Maximum	3,90 ± 0,08
			Minimum	1,71 ± 0,07

Measuments of the features in the each final COP stamps (rods, hexagons, and stars arrays):

Patterns	Rods	Hexagons	Stars	
Length (µm)	9,66 ± 0,08	9,43 ± 0,12	8,77 ± 0,12	
Width (µm)	2,35 ± 0,04	8,69 ± 0,13	7,78 ± 0,18	
Distance (µm)	1,09 ± 0,04	1,24 ± 0,08	Maximum	3,95 ± 0,04
			Minimum	1,96 ± 0,18

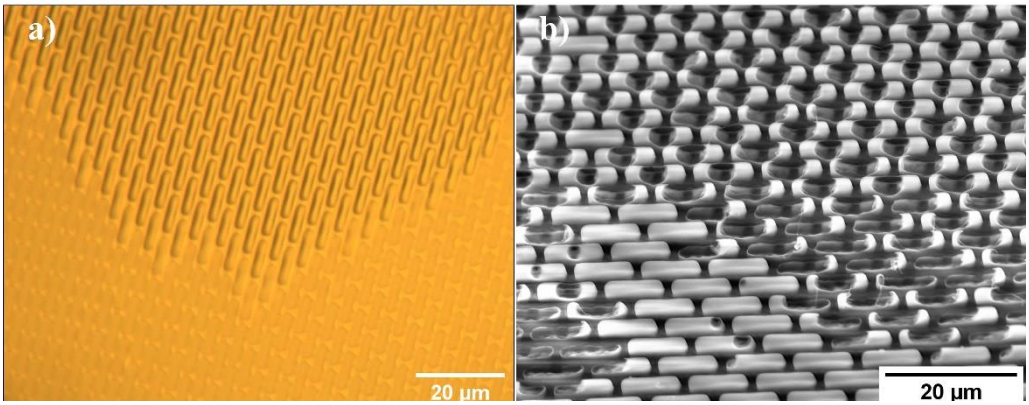

Figure 6 - Examples of poor stamp wetting. a) optical microscope image taken right after coating. b) SEM Tablet top micrograph after UV-assisted punching.

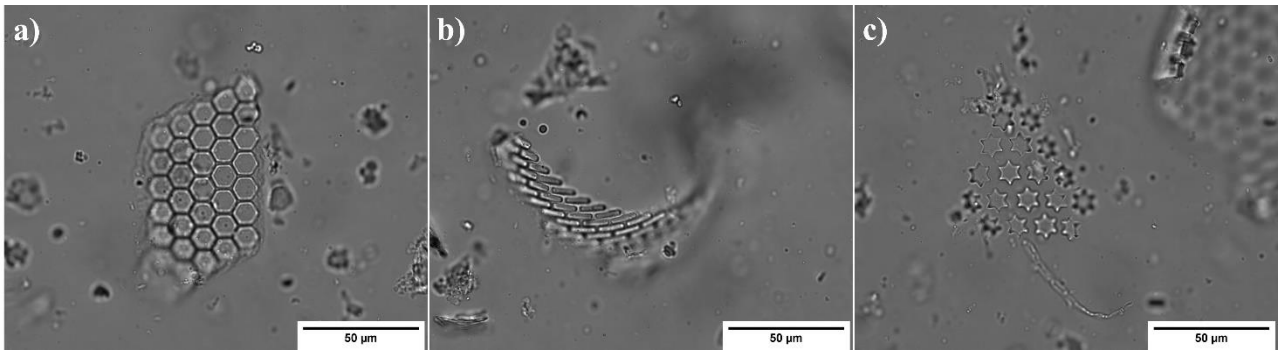

Figure 7 - Examples of microgel shapes connected through flash layer after PVA dissolution. a) hexagons, b) rods, and c) stars.

⟨2022⟩ Mariana Alves

Design and fabrication of microgel shapes as red blood cells (RBCs) substitutes by UV-assisted punching

NOVA SCHOOL OF SCIENCE & TECHNOLOGY